

# **Synthesis of MXene-based Nanocomposites for Supercapacitor Application**



By

Zoha Imran

(Registration No: 00000402070)

Department of Materials Engineering

School of Chemical and Materials Engineering

National University of Sciences & Technology (NUST)

Islamabad, Pakistan

(2024)

# **Synthesis of MXene-based Nanocomposites for Supercapacitor Application**



By

Zoha Imran

(Registration No: 00000402070)

A thesis submitted to the National University of Sciences and Technology, Islamabad,

in partial fulfillment of the requirements for the degree of

Master of Science in  
Nanoscience & Engineering

Supervisor: Dr. Iftikhar Hussain Gul

Co Supervisor: Dr. Sofia Javed

School of Chemical and Materials Engineering

National University of Sciences & Technology (NUST)

Islamabad, Pakistan

(2024)



## THESIS ACCEPTANCE CERTIFICATE

Certified that final copy of MS Thesis entitled "Synthesis of MXene-based Nanocomposites for Supercapacitor Application" written by Ms **Zoha Imran** (Registration No 00000402070), of School of Chemical & Materials Engineering (SCME) has been vetted by undersigned, found complete in all respects as per NUST Statues/Regulations, is free of plagiarism, errors, and mistakes and is accepted as partial fulfillment for award of MS degree. It is further certified that necessary amendments as pointed out by GEC members of the scholar have also been incorporated in the said thesis.

Signature: \_\_\_\_\_

Name of Supervisor: **Dr Iftikhar Hussain Gul**

Date: 06/01/2024

Signature (HOD): \_\_\_\_\_

Date: 07-01-25

Signature (Dean/Principal): \_\_\_\_\_

Date: 7/1/25

**National University of Sciences & Technology (NUST)**  
**MASTER'S THESIS WORK**

Formulation of Guidance and Examination Committee (GEC)

Name: Zoha Imran NUST Reg No: 00000402070  
 Department: Department of Materials Engineering Specialization: Master of Science in Nanoscience & Engineering  
 Credit Hour Completed: 18.0 CGPA: 3.33

**Course Work Completed**

S/No:	Code:	Title:	Core/Elective:	CH:	Grade:
1.	NSE-S13	Essentials of Nanoscience and Engineering	Compulsory	3.0	B
2.	MSE-854	Characterization Of Materials	Compulsory	3.0	B
3.	RM-898	Research Methodology	Additional	2.0	Q
4.	NSE-843	Nano Technology And Photovoltaics	Elective	3.0	B+
5.	MSE-856	Nano Material and Processing	Compulsory	3.0	B+
6.	NSE-941	Nano Composite Materials	Elective	3.0	B
7.	MSE-954	Advanced Characterization Techniques	Elective	3.0	A

Date: 31-Aug-2023

Student's Signature

**Thesis Committee**

Name: Iftikhar Hussain Gul (Supervisor)  
 Department: Department of Materials Engineering

Signature

Name: Sofia Javed (Cosupervisor)  
 Department: Department of Materials Engineering

Signature

Name: Zakir Hussain (Internal)  
 Department: Department of Materials Engineering

Signature

Name: Nasir Mahmood Ahmad (Internal)  
 Department: Department of Materials Engineering

Signature

Date: 31-Aug-2023

Signature of Head of Department:

**APPROVAL**

Date: 31-Aug-2023

Signature of Dean/Principal:



National University of Sciences & Technology (NUST)

FORM TH-4

MASTER'S THESIS WORK

We hereby recommend that the dissertation prepared under our supervision by

Regn No & Name: 00000402070 Zoha Imran

Title: Synthesis of MXene-based Nanocomposites for Supercapacitor Application.

Presented on: 19 Dec 2024 at: 1100 hrs in SCME

Be accepted in partial fulfillment of the requirements for the award of Masters of Science degree in Nanoscience & Engineering.

Guidance & Examination Committee Members

Name: Dr Nasir M. Ahmed

Signature: [Signature]

Name: Dr Zakir Hussain

Signature: [Signature]

Name: Sofia Javed (Co-Supervisor)

Signature: [Signature]

Supervisor's Name: Dr Iftikhar Hussain Gul

Signature: [Signature]

Dated: 19/12/2024

[Signature]  
Head of Department

24-12-24

Date

COUNTERSIGNED

[Signature] 26/12/24

Date \_\_\_\_\_

Dean/Principal

School of Chemical & Materials Engineering (SCME)

## **AUTHOR'S DECLARATION**

I Zoha Imran hereby state that my MS thesis titled "Synthesis of MXene-based Nanocomposites for Supercapacitor Application" is my own work and has not been submitted previously by me for taking any degree from National University of Sciences and Technology, Islamabad or anywhere else in the country/ world.

At any time if my statement is found to be incorrect even after I graduate, the university has the right to withdraw my MS degree.

Name of Student: Zoha Imran

Date: 11-10-2024

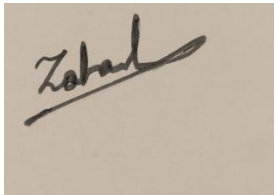
## **PLAGIARISM UNDERTAKING**

I solemnly declare that research work presented in the thesis titled “Synthesis of MXene-based Nanocomposites for Supercapacitor Application” is solely my research work with no significant contribution from any other person. Small contribution/ help wherever taken has been duly acknowledged and that complete thesis has been written by me.

I understand the zero-tolerance policy of the HEC and National University of Sciences and Technology (NUST), Islamabad towards plagiarism. Therefore, I as an author of the above titled thesis declare that no portion of my thesis has been plagiarized and any material used as reference is properly referred/cited.

I undertake that if I am found guilty of any formal plagiarism in the above titled thesis even after award of MS degree, the University reserves the rights to withdraw/revoke my MS degree and that HEC and NUST, Islamabad has the right to publish my name on the HEC/University website on which names of students are placed who submitted plagiarized thesis.

Student Signature:

A rectangular box containing a handwritten signature in black ink. The signature appears to be 'Zoha Imran' written in a cursive style.

Name: Zoha Imran

## **DEDICATION**

*I dedicate this thesis to the growth I made during this journey and all the people that were part of it.*



## **ACKNOWLEDGEMENTS**

First and foremost, I would like to thank Allah Almighty for giving me the courage to start and complete this research, and for providing the strength to overcome all obstacles.

I would like to express my sincere gratitude to my supervisor, Prof. Dr. Ifthikhar Hussain Gul, for his invaluable guidance and insightful feedback throughout my research journey. His considerable experience and knowledge really pushed me to do better. I whole-heartedly appreciate his patience and the opportunities that he gave me for my academic growth.

I would like to thank my co-supervisor, Dr. Sofia Javed, for her support and guidance. I appreciate the knowledge that I gained from her. I would also like to thank my GEC members, Dr. Zakir Hussain and Dr. Nasir Mehmood Ahmad, for their guidance.

I would like to express my deepest gratitude to my friends, Haleema Sultan Akbar, Vania Sayyab, Fareeha Batool and Khadija Sultan for their unwavering support and inspiration. Their immense moral support really kept me going throughout my research journey.

Finally, I would like to thank my family, my mother, my father, my sister Areej Imran and my brother Zain Imran, for their love and unconditional support.

**Zoha Imran**

# TABLE OF CONTENTS

<b>ACKNOWLEDGEMENTS</b>	<b>IX</b>
<b>TABLE OF CONTENTS</b>	<b>X</b>
<b>LIST OF TABLES</b>	<b>XIII</b>
<b>LIST OF FIGURES</b>	<b>XIV</b>
<b>ABSTRACT</b>	<b>XVI</b>
<b>CHAPTER 1: INTRODUCTION</b>	<b>1</b>
<b>1.1 Renewable Energy Sources</b>	<b>1</b>
<b>1.2 Energy Storage Devices</b>	<b>1</b>
1.2.1 Batteries and Supercapacitors	2
1.2.2 Batteries vs. Supercapacitors	3
<b>1.3 Supercapacitors</b>	<b>4</b>
1.3.1 Types of Supercapacitors	5
1.3.2 Electrostatic Double Layer capacitors	6
1.3.3 Pseudocapacitor	7
1.3.4 Hybrid Supercapacitors	7
1.3.5 Applications of Supercapacitors	8
1.3.6 Challenges in Supercapacitors	9
<b>1.4 Electrode Material</b>	<b>9</b>
1.4.1 Types of Electrode Materials	9
1.4.2 Carbon based materials	10
1.4.3 Metal Oxides	10
1.4.4 Polymer based materials	10
1.4.5 Challenges in Electrode Materials	11
<b>1.5 MXene</b>	<b>11</b>
1.5.1 MXene as an Electrode Material	13
1.5.2 Challenges in MXene	13
<b>1.6 Biomass as Renewable Carbon Source</b>	<b>13</b>
1.6.1 Activated Carbon as Electrode material	15
1.6.2 Challenges in Activated Carbon	15
<b>1.7 Research Objectives</b>	<b>16</b>
<b>CHAPTER 2: LITERATURE REVIEW</b>	<b>17</b>
<b>2.1 Supercapacitors for Energy Storage</b>	<b>17</b>
<b>2.2 Conventional Electrode Material</b>	<b>18</b>
2.2.1 Carbon based Materials	18
2.2.2 Metal Oxide based Electrode Materials	19

2.2.3 Conducting Polymer Based Electrode Materials	20
<b>2.3 2D Material as Electrode Material for Supercapacitors</b>	<b>21</b>
2.3.1 Graphene	22
2.3.2 Transition metal dichalcogenides (TMDs)	22
2.3.3 Metal-organic frameworks (MOFs)	23
<b>2.4 MXene: Structure and Composition</b>	<b>23</b>
2.4.1 HF Etching	24
2.4.2 Alkali Etching	25
2.4.3 Electrochemical Etching	25
<b>2.5 MXene as Electrode for Supercapacitors</b>	<b>26</b>
<b>2.6 Biomass derived Carbonaceous Materials</b>	<b>27</b>
2.6.1 Precursors for Biomass derived Carbonaceous Materials	27
2.6.2 Pyrolysis	28
2.6.3 Hydrothermal Carbonization	29
2.6.4 Activation	29
<b>2.7 Activated Carbon as Electrode Material for Supercapacitor</b>	<b>30</b>
<b>CHAPTER 3: MATERIALS AND METHODS</b>	<b>39</b>
<b>3.1 Materials</b>	<b>39</b>
<b>3.2 Synthesis of MXene (Ti<sub>3</sub>C<sub>2</sub>T<sub>x</sub>)</b>	<b>39</b>
<b>3.3 Synthesis of Activated Carbon</b>	<b>40</b>
<b>3.4 Synthesis of MXene/Activated Carbon Composite</b>	<b>41</b>
<b>3.5 Electrode Preparation</b>	<b>42</b>
<b>CHAPTER 4: CHARACTERIZATION</b>	<b>44</b>
<b>4.1 X-ray diffraction (XRD)</b>	<b>44</b>
<b>4.2 Raman Spectroscopy</b>	<b>45</b>
<b>4.3 Scanning Electron Microscope (SEM)</b>	<b>46</b>
4.3.1 Principle of SEM	47
<b>4.4 BET Surface Area Analysis</b>	<b>48</b>
4.4.1 Sample Preparation for BET	49
4.4.2 Instrumentation of BET	49
<b>4.5 Electrochemical Measurement</b>	<b>50</b>
4.5.1 Cyclic Voltammetry	50
4.5.2 Galvanostatic Charge-Discharge Analysis	51
4.5.3 Cyclic Stability	52
4.5.4 Electrochemical Impedance Spectroscopy	52
<b>CHAPTER 5: RESULTS AND DISCUSSION</b>	<b>54</b>
<b>5.1 XRD analysis</b>	<b>54</b>
<b>5.2 Raman analysis</b>	<b>55</b>
<b>5.3 Brunauer Emmett Teller analysis</b>	<b>57</b>
<b>5.4 SEM analysis</b>	<b>58</b>
<b>5.5 Electrochemical Characterization</b>	<b>60</b>
<b>5.6 Cyclic Voltammetry (CV)</b>	<b>60</b>
<b>5.7 Galvanostatic Charge Discharge (GCD)</b>	<b>64</b>
<b>5.8 Electrochemical impedance Spectroscopy (EIS)</b>	<b>66</b>

<b>5.9</b>	<b>Cycle Stability</b>	<b>68</b>
<b>CHAPTER 6:</b>	<b>CONCLUSION</b>	<b>70</b>
<b>REFERENCES</b>		<b>72</b>

## LIST OF TABLES

	<b>Page No.</b>
Table 1: Comparison of supercapacitor and battery [5].....	3
Table 2: Specific capacitance of all samples calculated from CV data. ....	63

# LIST OF FIGURES

	<b>Page No.</b>
Figure 1: Ragone plot for energy storage devices [4].....	2
Figure 2: Supercapacitor [9]. .....	5
Figure 3: Types of supercapacitors [10]. .....	5
Figure 4: Working mechanism of different types of supercapacitors [11]. .....	6
Figure 5: Working of an EDLC [13].....	7
Figure 6: Charge storage mechanism of a pseudocapacitor [15].....	7
Figure 7: Mechanism of charge storage in a hybrid supercapacitor [17]. .....	8
Figure 8: MXene structure and composition [30].....	13
Figure 9: Biomass as renewable carbon source [39]. .....	14
Figure 10: Biomass derived activated carbon as supercapacitor electrode [42]. .....	15
Figure 11: MAX phase to MXene [78].....	24
Figure 12: Synthesis process of MXene. ....	40
Figure 13: Synthesis of biomass derived activated carbon. (a): Carbonization Process. ....	40
Figure 14: Synthesis process of MXene/AC composites.....	42
Figure 15 : Electrode preparation process .....	43
Figure 16: Mechanism of XRD [96]. .....	45
Figure 17: Working of Raman [98]. .....	46
Figure 18: Working principle of SEM [100]. .....	47
Figure 19: Mechanism of BET analysis [102].....	49
Figure 20: BET equipment [103].....	50
Figure 21: Three electrode based electrochemical cell set up and cyclic voltammogram [104]..	51
Figure 22: GCD curves of (a) EDLC (b)Pseudo capacitor [105]. .....	52
Figure 23: EIS (a) Equivalent circuit diagram (b)Nyquist plot [106].....	53
Figure 24: XRD pattern of MXene, AC, MAC1, MAC2 and MAC3. ....	55
Figure 25: Raman plots of MXene. AC, MAC1, MAC2 and MAC3.....	57
Figure 26: BET plot of MXene, AC, MAC1, MAC2 and MAC3. ....	58
Figure 27: SEM images of (a) MXene, (b) AC, (c) MAC1, (d) MAC2 and (e) MAC3.....	60
Figure 28: Cyclic voltammograms of (a) all samples at 5mV/s, (b) MXene at various scan rates, (c) AC at various scan rates, (d) MAC1 at various scan rates, (e) MAC2 at various scan rates and (f) MAC3 at various scan rates. ....	63
Figure 29: GCD curves of (a) All samples at 1 A/g, (b) MXene at different current densities, (c) AC at different current densities, (d) MAC1 at different current densities, (e) MAC2 at different current densities, (f) MAC3 at different current densities. ....	66
Figure 30: Nyquist plots of MXene, AC, MAC1, MAC2 and MAC3.....	67
Figure 31: Bode phase angle plot of MXene, AC, MAC1, MAC2 and MAC3.....	68
Figure 32: Cycle stability and Coulombic efficiency plot of MAC3.....	69

## LIST OF ABBREVIATIONS

AC	Activated Carbon
MAC	MXene/activated carbon composite
SC	Supercapacitor
CV	Cyclic Voltammetry
GCD	Galvanostatic charge discharge
EIS	Electrochemical impedance spectroscopy
SEM	Scanning electron microscopy
XRD	X-ray diffraction
BET	Brunauer Emmett Teller

## ABSTRACT

Two-dimensional multilayered MXene is a promising electrode material for supercapacitor application. Studies have revealed that using MXene as electrode material in supercapacitors yields a high specific capacitance and enhanced electrochemical performance. However, the two-dimensional structure of MXene nanosheets are prone to self-restacking due to Van der Waals forces, which decreases the active sites for ion adsorption-desorption, thereby limiting its electrochemical properties. We devised a strategy to overcome this issue, by making a composite of MXene with activated carbon (AC) can not only prevent aggregation of MXene sheets, but the porous structure of AC can also provide abundant channels for rapid electrolyte ion transport. Biomass derived activated carbon was successfully synthesized by KOH activation method. It not only showed superior electrochemical properties but is also a cost-effective and sustainable alternative to other carbon materials. The synthesized MXene/AC composites demonstrated excellent electrochemical performance which is ascribed to the high porosity and surface area offered by activated carbon, and the synergistic effect of excellent conductivity of MXene and biomass derived activated carbon. XRD pattern confirmed the successful synthesis of MXene, AC and their composites. Raman revealed that degree of disorder increases, and degree of graphitization decreases with increase in AC content in MXene. BET analysis showed a similar trend, an increase in the surface area of the composites with an increased amount of AC. SEM showed the successful transformation of MXene from MAX phase, porous structure of AC and a 2D/3D conductive network of MXene/AC composites. Electrochemical analysis revealed MAC3 exhibited a high specific capacitance of 1080 F/g at 5 mV/s, outperforming both MXene and activated carbon. MAC3 also displayed a good cyclic stability of 81.1% and a Coulombic efficiency of 98.5% after 300 cycles. These results indicate that the synthesized MXene/AC composite can be used as an efficient electrode material for enhanced performance of supercapacitors.

**Keywords:** MXene, Biomass, Activated carbon, Supercapacitors, Electrode material, MXene/Activated carbon composite.



# **CHAPTER 1: INTRODUCTION**

## **1.1 Renewable Energy Sources**

Due to factors like climate change, increased urbanization, industrialization, and population growth, the global energy demand is growing at an alarming rate. The global energy sector is significantly impacted by fossil fuels. The extensive use of fossil fuels is causing several natural disasters, including greenhouse gas emissions, global warming, and other adverse effects. Therefore, the need for the development of sustainable energy sources is becoming more crucial [1]. Consequently, a growing number of researchers worldwide are focusing on lowering the use of fossil fuels and employing alternative energy sources like solar, geothermal and wind energy which are more sustainable.

## **1.2 Energy Storage Devices**

Energy storage refers to the accumulation of energy within certain devices or systems for subsequent use at the time of need. The development of sustainable, innovative, and cost-effective energy storage devices is essential to address the environmental issues of modern society. For this, devices like batteries, supercapacitors and fuel cells are being developed [2]. To make these devices cost effective and more efficient, thorough research is required. The predominant energy storage technologies in electrical and electrochemical systems are supercapacitors and batteries [3].

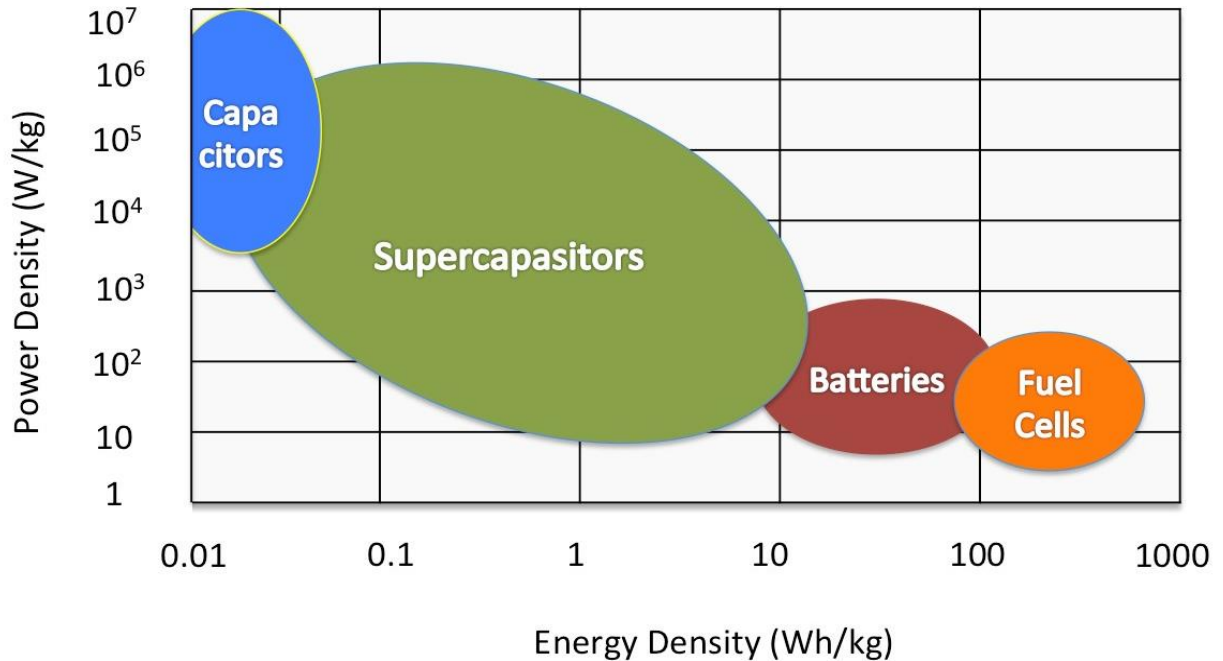


Figure 1: Ragone plot for energy storage devices [4].

### 1.2.1 Batteries and Supercapacitors

In recent years there hasn't been as much research into supercapacitors as there has been into batteries. However, supercapacitors have properties which make them suitable for many applications. For instance, they can offer ten times more power than batteries. With a longer cycle life, supercapacitors have a rapid rate of charging and discharging. These characteristics enable supercapacitors, particularly redox supercapacitors, to replace batteries in various applications. Because of its technique for storing charge, redox supercapacitors have superior characteristics to those of regular batteries [1].

Currently, rechargeable batteries including lithium-sulfur, lithium-ion and lead-acid are available. Batteries mostly store charge through enormous diffusion or through the insertion and disinsertion of cations. The electrode material experiences compositional and phase changes because of cation insertion/disinsertion and bulk diffusion. Due to the diffusion control mechanism, this method is slow and has a limited power density, or charge-discharge rate [1]. Cations flow via the van der Waal gaps when the electrode material is in layered form, as in pseudocapacitive materials. Cations can also be electrochemically adsorbed on

electrode material's surface through a process of charge transfer. Metal atoms are reduced when they are adsorbed on a surface or when they go into the lattice planes. Charges are quickly absorbed at the surface, but they travel slowly into the interlayer lattice planes. As cations have been seen to readily diffuse into the Van der Waal gap, this phenomenon—also referred to as intercalation pseudo capacitance—can be regarded as capacitive. This technique is pseudocapacitive because faradic storage of cations does not alter the phase or composition of the electrode material. In comparison to bulk diffusion phenomena, the rate of cation storage by pseudocapacitive method is faster [1].

Table 1: Comparison of supercapacitor and battery [5].

<b>Characteristics</b>	<b>Supercapacitors</b>	<b>Batteries</b>
Power density (W/kg)	10,000	50–200
Energy density (Wh/kg)	1–20	20–100
Charge/Discharge	≈100 %	Less than 85 %
Equivalent series resistance	Typically, in mΩ range	Fractional Ω to few Ω
Cycle time	50,000–1,000,000	500–2000
Charge time	1–60 s	3600–18,000 s
Discharge time	0.1–30 min	10–180 min

### *1.2.2 Batteries vs. Supercapacitors*

The main difference between batteries and supercapacitors is the various changes in composition and phases that occur during the battery's charge and discharge cycles. Because diffusion controls the process and batteries primarily store charge through bulk diffusion, it slows down and reduces the power density, or charge discharge rate. On the other hand, because cations are stored faradaically in supercapacitors and the phases and composition of the electrode material remain unchanged, cation storage occurs quickly there. The reaction in supercapacitors is kinetically controlled and happens more quickly across the time scale of interest than diffusion-controlled processes in batteries. The type of energy storage system to use is determined by the speed of the storage process and the amount of energy required by the application. Capacitors are used in applications that need a higher discharge rate, while batteries are used in applications that need a slower discharge rate [6].

### 1.3 Supercapacitors

Supercapacitors are a kind of electrochemical energy storage device with high specific capacitance and power density [7]. Supercapacitors have drawn a lot of interest in recent years because of their low-cost, high-power density, extended cycle life, and quick charge and discharge rates. Supercapacitors are a kind of electrochemical energy storage devices with high specific capacitance, low-cost, high-power density, extended cycle life, and quick charge and discharge rates [7]. Supercapacitors have a wide range of uses because of these characteristics, including hybrid electric cars and portable gadgets etc.

Supercapacitors are made up of two electrodes, an electrolyte and a porous membrane separator. This specific structure of supercapacitors makes them have the features of conventional capacitors as well as electrochemical batteries. A supercapacitor works by drawing opposing charge carriers from the electrolyte to its electrodes when a potential difference is applied across its terminals. At the negative terminal, positive ions concentrate, whereas at the positive terminal, negative ions do the same. Charge carriers are stored on the current collector plates. An electrostatic field forms between the current collectors because of the accumulation of opposing charges. Until the electrostatic field between the current collectors equals and is opposite to the supplied voltage, charging current flows through the capacitor. The charge carriers are held by the current collectors until the applied voltage drops or changes polarity. A certain amount of charge carriers are returned to the electrolyte from the current collectors whenever the applied voltage drops. A comparable current travels through the capacitor in the opposite direction throughout this procedure. The supercapacitor experiences a similar cycle of charging and discharging when the polarity changes [8].



Figure 2: Supercapacitor [9].

### 1.3.1 Types of Supercapacitors

They are divided into three types based on their charge storage mechanism.

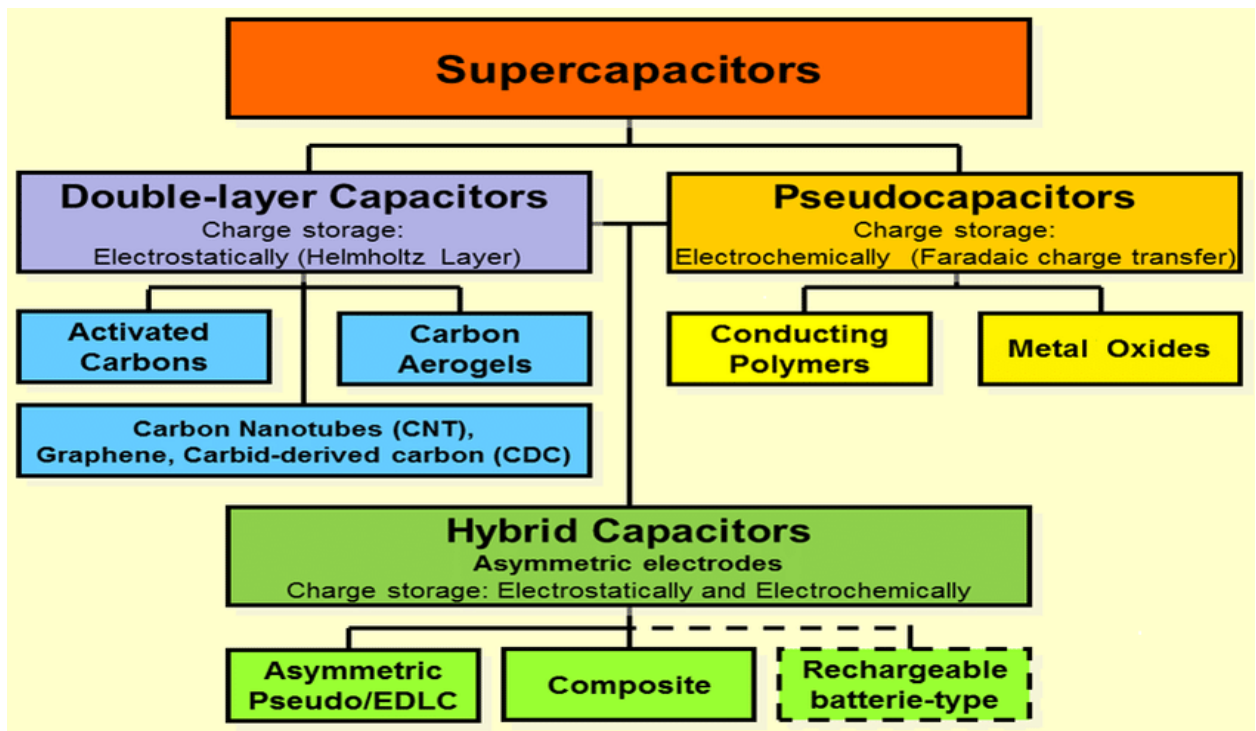


Figure 3: Types of supercapacitors [10].

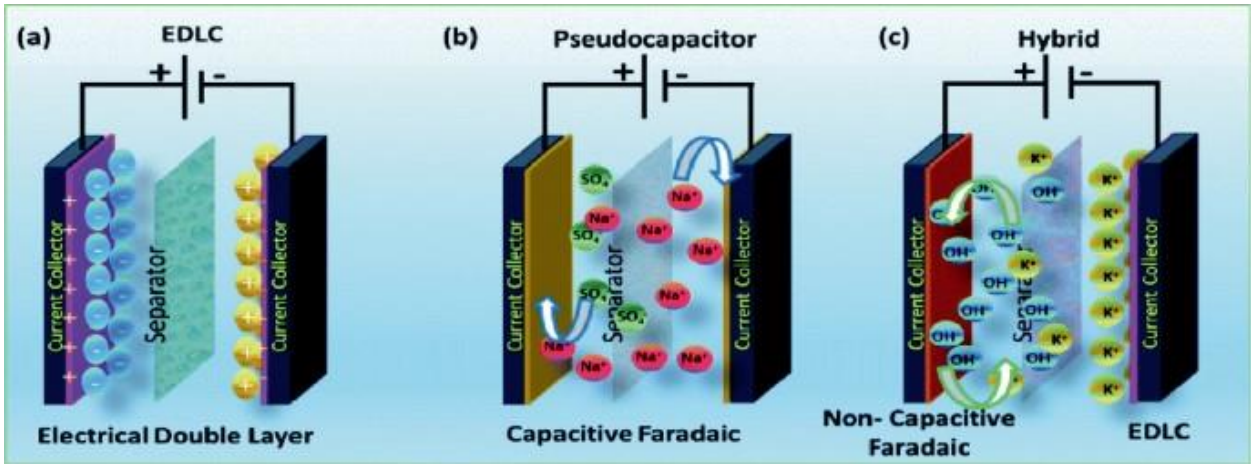


Figure 4: Working mechanism of different types of supercapacitors [11].

### 1.3.2 Electrostatic Double Layer capacitors

This kind of capacitor works by generating an electrical double layer, which allows a charge to be physically held on the electrode surface without resulting in any irreversible chemical reactions. Mostly carbon-based electrodes are used in this type of supercapacitors, which are spaced by an insulating material called a dielectric, which also has electrical characteristics that can impact the supercapacitor's performance [6]. Supercapacitors store charges electrostatically. As soon as a voltage is applied across the terminals, an electric field is created at each electrolyte, causing the electrolyte to polarize. This causes ions to diffuse to the porous electrodes of opposing charges through the dielectric. Each electrode experiences the creation of an electric double layer in this manner. As a result, each electrode's surface area increases while the space between them decreases [12].

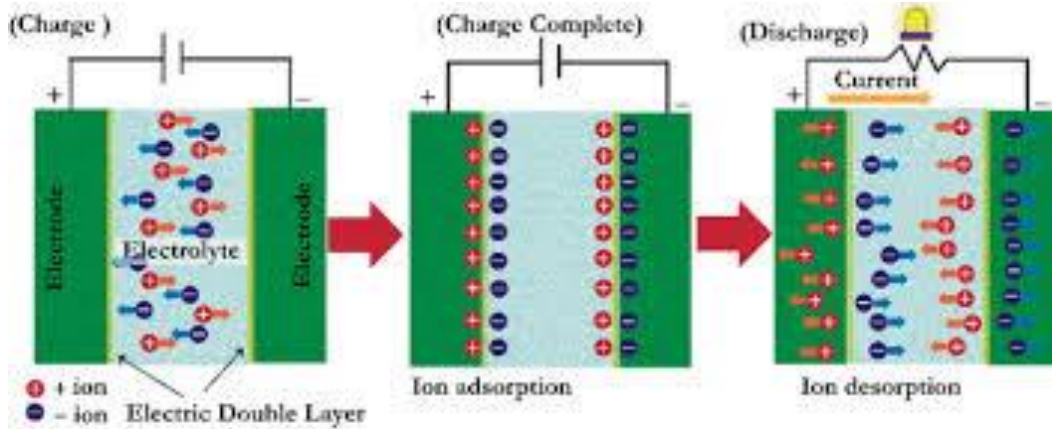


Figure 5: Working of an EDLC [13].

### 1.3.3 Pseudocapacitor

Pseudo-capacitors are also referred to as faradic supercapacitors. These devices use electrodes made of redox-active materials such as conductive polymers and metal oxides [14]. These electrodes store charge close to each other or at the electrode surface through a reversible Faraday reaction mechanism in which the charge is transported across the metal-electrolyte interface.

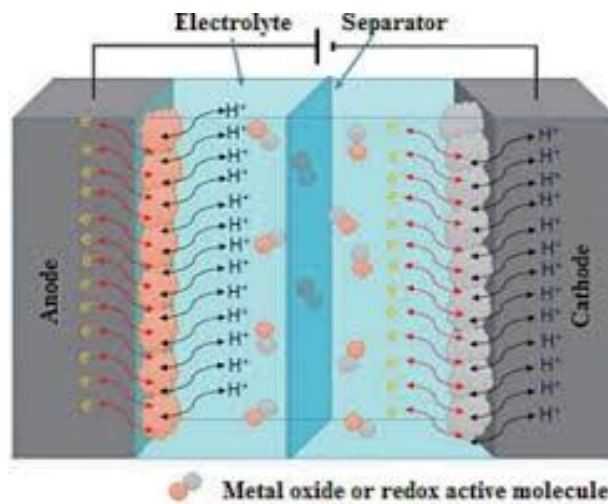


Figure 6: Charge storage mechanism of a pseudocapacitor [15].

### 1.3.4 Hybrid Supercapacitors

These capacitors use both pseudocapacitor and EDLC processes. Hybrid capacitors consist of electrodes with different properties based on chemical and electrical mechanisms. Thus, one electrode provides an electrostatic capacity while the other electrode has an electrochemical capacity. Benefits include increased operating voltage, energy density and capacity [16].

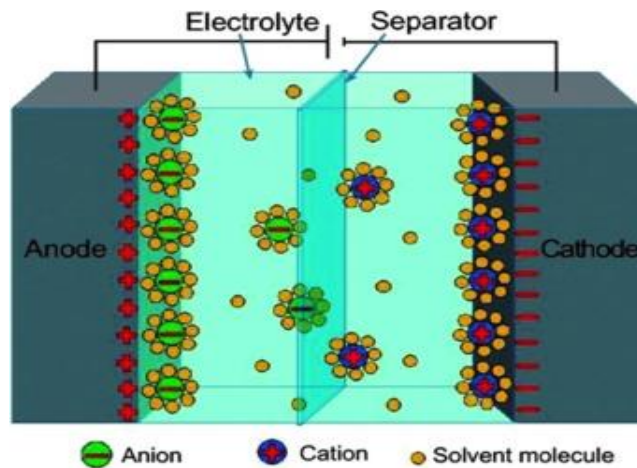


Figure 7: Mechanism of charge storage in a hybrid supercapacitor [17].

### 1.3.5 Applications of Supercapacitors

Due to their unique storage capabilities, supercapacitors have extensive applications, such as:

- Supercapacitors are being used in automobiles to supply stored energy in a matter of seconds, and their use in the field of energy-efficient services is growing quickly [18].
- Supercapacitors are even used in renewable energy sources such as wind energy to control blade pitch.
- Supercapacitors are used to create memory devices found in computers, tablets, cellphones, and other gadgets. They are also utilized in LED flash devices.
- In the transportation industry, supercapacitors are employed in hybrid buses because they work in tandem with the battery to extend its lifespan and reduce its volume.



### *1.3.6 Challenges in Supercapacitors*

Supercapacitors face problems such as low energy density, low single cell voltage, excessive self-discharge and poor capacity. While still having a smaller capacitance than batteries and fuel cells, supercapacitors have a greater capacitance than regular capacitors. To address the low capacitance problem, electrode material can be composed of many innovative materials and used in supercapacitors [19]. The choice of electrode material is very important in supercapacitors because it affects the electrical properties. New electrode materials for supercapacitors should have high specific surface area, large pore size, strong conductivity, customizable shape, permeability to electrolyte solutions and good surface functionality to increase capacity. One of the top priorities is to design electroactive materials with improved electrochemical properties. The most important thing to do is to create electrodes made of such materials that have a high electron capture and storage capacity [19].

## **1.4 Electrode Material**

The supercapacitor's electrode material is its most crucial component. The type and properties of this material determine the performance of a supercapacitor in terms of total mass, operating voltage and storage capacity [20]. The type of charge storage mechanism depends on the type of electrode material, with rapid reversible Faraday reactions at the electrode surface leading to pseudocapacitor behavior and electrostatic attraction between the two electrodes leading to EDLC behavior. The charge storage ability of a supercapacitor greatly depends on the accessible surface area of the electrode. In general, electrode materials with high power density, excellent cycle life, long cycle stability and high Coulombic efficiency are the ideal choice for supercapacitors [20].

### *1.4.1 Types of Electrode Materials*

High-performance supercapacitors are the outcome of using nanostructured materials. A material's surface area is crucial since it has a big impact on capacitive

performance. High pore volume and porosity in nanomaterials contribute to the material's high capacitance. The three main categories of electrode materials are listed below.

- Carbon based materials.
- Metal oxides.
- Polymer based materials.

#### *1.4.2 Carbon based materials*

Supercapacitors have used a variety of carbonaceous materials as their electrodes, including carbon nanotubes (CNTs), carbon nano fibers (CNF), porous carbon, graphene [21]. These electrode materials offer unique advantages such as, good electronic conductivity, high chemical and thermal stability, hierarchical porous structure, wide working temperature range as well as easy manufacturing and cost effectiveness. Pure carbon compounds electrostatically store charges to generate electric double-layer capacitance (EDLC) [22].

#### *1.4.3 Metal Oxides*

In MO-based Supercapacitors, a variety of metal oxides, including manganese oxide ( $\text{MnO}_2$ ), nickel oxide (NiO), cobalt oxide ( $\text{Co}_3\text{O}_4$ ) and ruthenium oxide ( $\text{RuO}_2$ ), are typically utilized as electrode materials. Because of their high specific capacitance and strong cycling stability, MO-based materials enable oxide-based supercapacitors to withstand multiple cycles of charging and discharging without experiencing deterioration [23]. This attribute is vital for the long-term reliability and durability of the supercapacitors. When the MO electrode encounters the electrolyte, a pseudo-capacitance mechanism is employed by metal oxide-based SCs to store energy. They are advantageous for applications requiring high power and energy storage capacities because reversible redox processes take place at the interface between the electrode and electrolyte, thereby storing charge exceeding the electrostatic double-layer capacitance.

#### *1.4.4 Polymer based materials*

Conducting polymers including, polyaniline, polythiophene, poly [3,4-ethylenedioxythiophene] and polypyrrole have been extensively researched because of their high electrical conductivity, environmental resilience and low cost [24]. When compared to other electrode materials, conductive polymer gained a lot of attention since they are relatively easy to process and flexible. Furthermore, the expansion and contraction of conducting polymers will be influenced by charges and ions because of the implantation and release of charged ions in the charging and discharging systems [19]. The electrode material's cycle stability performance is frequently deteriorated by this process.

#### *1.4.5 Challenges in Electrode Materials*

The challenges faced by electrode materials include low specific surface area, low electrical conductivity, low ionic conductivity, self-discharge, chemical stability, and low mechanical strength [25]. All these factors influence electrode material's overall performance. Therefore, the key to improving the electrochemical performance of electrode materials lies in developing a material that improves the above parameters.

### **1.5 MXene**

MXenes, a family of two-dimensional (2D) atomic-thick materials made from transition metal carbides, nitrides, or carbonitrides—have gained popularity since their discovery in 2011 by Naguib et al. has attracted considerable attention in recent years. Mxene has the chemical formula  $M_{n+1}X_n$  ( $n = 1-3$ ), where X represents carbon or nitrogen and M is an early transition metal such as titanium, tantalum or niobium.  $M_{n+1}AX_n$ , where M is an early transition metal, A is an element of the IIIA or IVA group, basic 3D forebody [26]. A-layers are stacked alternately between  $M_{n+1}AX_n$  units in a multilayer hexagonal structure, which appears to characterize the MAX phase. Since the M-X bond is mainly composed of covalent and ionic bonds, the M-X bond is much stronger than the metallic bond of M-A, so the M-A layer bond is relatively weak and therefore the layer can potentially be separated from the MAX phase. Removal of the A layer leads to the formation of MXene, which can be expressed as  $M_{n+1}X_nT_x$ , where  $T_x$  represents surface termination, meaning MXene has good electrical conductivity due to its

inherent 2D atomic structure, layered structure, metallic conductivity, electronic properties, plasmonic properties, optical properties, chemical stability, hydrophilicity and high aspect ratio. Due to these properties, MXene is of interest for various applications such as energy storage, EMI shielding, biosensing, catalysis, antibacterial activity, sensors and optoelectronics [27]. Multiple forms of MXenes exist [28]:

- Solid solution MXenes (e.g.,  $\text{Mo}_{4-y}\text{VyC}_3\text{T}_x$ ,  $\text{Ti}_{2-y}\text{VyCT}_x$ ,  $\text{Ti}_{2-y}\text{NbyCT}_x$ )
- Ordered double transition metal MXenes (e.g.,  $\text{Mo}_2\text{TiC}_2\text{T}_x$ ,  $\text{Cr}_2\text{TiC}_2\text{T}_x$ )
- Ordered divacancy MXenes ( $\text{W}_{1.33}\text{CT}_x$ , etc.)
- Ordered double transition metal MXenes (e.g.,  $\text{Mo}_2\text{TiC}_2\text{T}_x$ ,  $\text{Mo}_2\text{Ti}_2\text{C}_3\text{T}_x$ ,  $\text{Cr}_2\text{TiC}_2\text{T}_x$ )
- Single metal element structures (e.g.,  $\text{Ti}_2\text{CT}_x$ ,  $\text{Ti}_3\text{C}_2\text{T}_x$ ,  $\text{V}_2\text{CT}_x$ , etc.)

Titanium carbide MXene has received more attention than other MXenes. Many variables, including simple synthesis process, layered structure, large flake size, excellent conductivity, raw material availability and, most importantly, long-term stability, have been attributed to  $\text{Ti}_3\text{C}_2\text{T}_x$  MXene's explosive growth in usage [29].  $\text{Ti}_3\text{C}_2\text{T}_x$  MXenes have great potential as supercapacitor electrode materials as well.

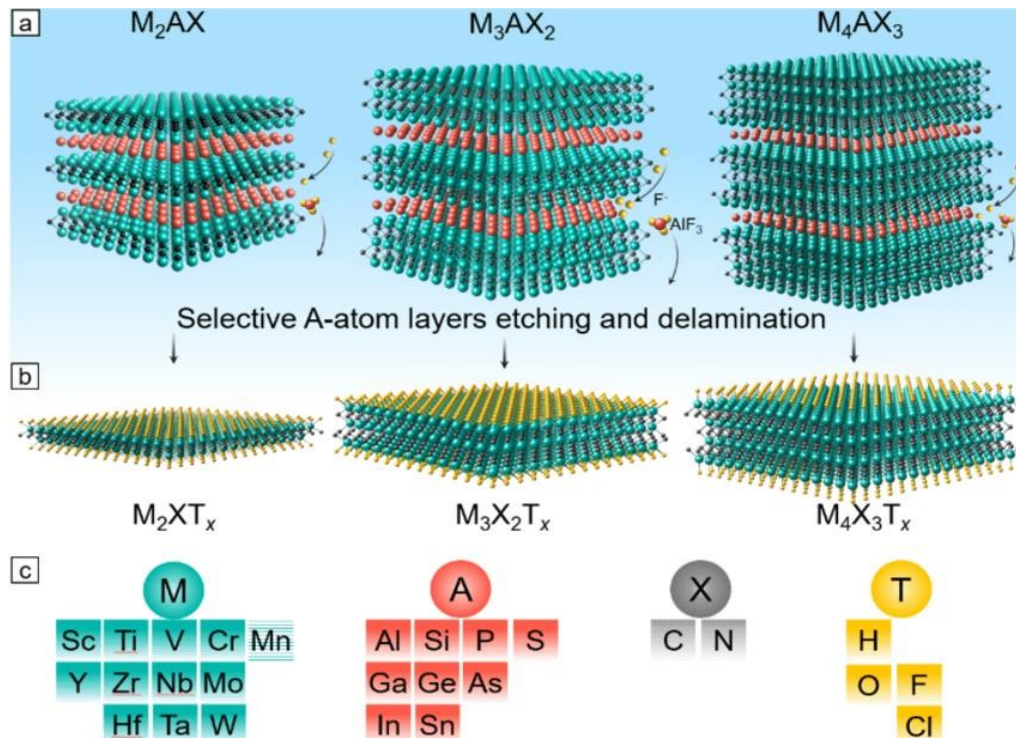


Figure 8: MXene structure and composition [30].

### *1.5.1 MXene as an Electrode Material*

Because of their unusual two-dimensional structure, programmable surface terminations, superior mechanical qualities, high density, quasi-metallic conductivity, MXenes provide special benefits as electrode material for supercapacitors [31]. Lukatskaya et al. [32] finally discovered the pseudocapacitive effect of  $Ti_3C_2T_x$  MXene. In 2013, this opened the door for application in supercapacitors and resulted in volume specific capacitance of up to 442 F/cm<sup>3</sup>. As research progresses, MXene has emerged as a potential electrode material.

### *1.5.2 Challenges in MXene*

The performance of MXene as an electrode material is limited due to agglomeration, and MXene nanosheets are also prone to stacking due to the strong van der Waals forces between layers. This results in multilayer structures that are prone to spontaneous collapse and have low energy density during early cycles, which in turn reduces the active sites available for electrolyte ions and thus reduces the electrochemical performance of the material [33]. To address this issue and improve the electrochemical performance of MXene, spacer materials must be used between MXene sheets to prevent re-stacking and agglomeration.

## **1.6 Biomass as Renewable Carbon Source**

The use of biomass has become popular as a fantastic replacement for depleting natural resources like fossil fuels and it has many advantages such as sustainability, cost effectiveness and renewability. It refers to materials originating from plants or animals and usually regarded as waste [34]. Worldwide, each year over 181 billion tonnes of biomass waste are produced [35]. Since it is naturally renewable, using it to produce chemicals, fuels, and functional materials is very attractive. Biomass resources such as wheat husk, wheat flour, rice husk, peanut shells, banana peels, apples, coconut shells etc., have been used to derive various carbonaceous materials. The efficient use of this biomass has been studied using various techniques ranging from bioconversion to thermochemical conversion. Thermochemical conversions include processes in which thermal degradation to gaseous, solid or liquid products predominates.

Common thermochemical methods for converting biomass into fuels and biochemicals include gasification, pyrolysis and hydrothermal conversion. During these processes, a sizable amount of biochar is formed [36]. Biochar is a carbon-rich solid produced by thermochemical conversion of biomass under oxygen-limited conditions. Physical activation or chemical activation are two ways to expand the surface area of biochar. Biochar is physically activated by heating it to 600-900 degrees Celsius and treating it with ammonia, carbon dioxide or a certain amount of air [37]. These activating gas streams reacts with the atoms of carbon present on the biochar's surface. Mesopores and micropores are produced when the carbon and activation agent continue to react. To chemically activate biochar, it must be treated at a temperature between 450 and 900 °C with acids, bases, metal salts, etc [37]. Activating agents like KOH, NaOH, H<sub>3</sub>PO<sub>4</sub> and ZnCl are frequently utilized [37]. Biochar is created by chemical activation, which results in a definite pore size distribution and new surface functions that are controllable based on the activating agent and process parameters. Furthermore, the porosity growth is significantly influenced by the ratio of activating agent to biochar. Biochar has unique physical and chemical properties, including high porosity, high surface area, stability, high electrical conductivity, presence of functional groups, and cation exchange capacity [38]. Due to these unique properties, carbonaceous materials derived from biomass are used in various applications such as energy storage, environmental remediation and biomedical sciences. Biomass-derived carbonaceous materials include activated carbon, heteroatom-doped carbonaceous material, biomass-derived graphene, porous carbon materials and carbon nanotubes.

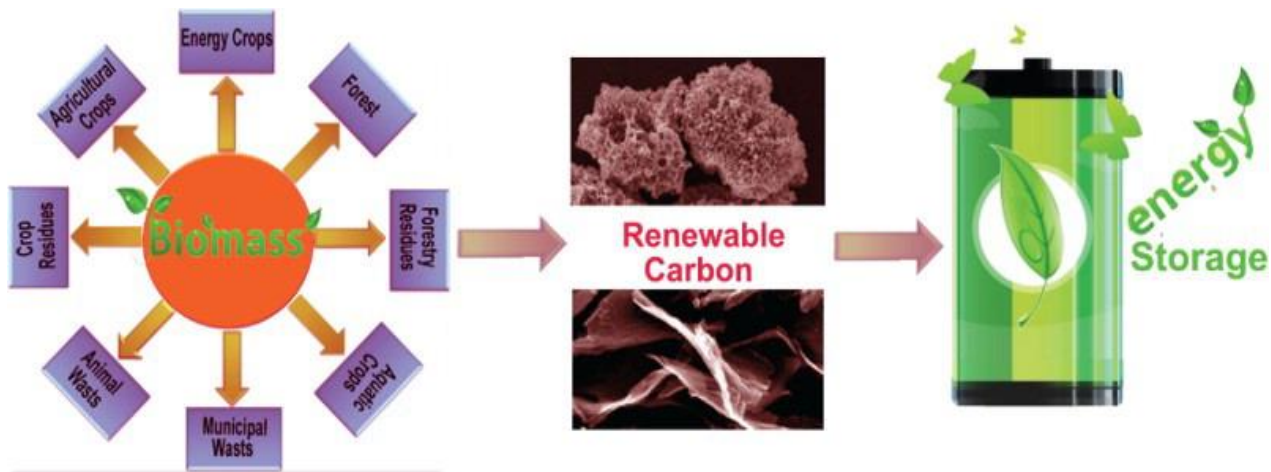


Figure 9: Biomass as renewable carbon source [39].

### 1.6.1 Activated Carbon as Electrode material

One of the most suitable materials for supercapacitor electrode applications is activated carbon. Compared to other carbon-containing materials, activated carbon has adjustable pore size and high specific surface area, these properties make activated carbon a popular choice as an electrode material for supercapacitors [40]. The layered pore structure, large surface area and unique morphology allows the formation of an ionic double layer at the electrode-electrolyte interface. This improves the overall performance of activated carbon used as an electrode material in supercapacitor applications. Additionally, activated carbon derived from biomass has a highly porous structure which provides abundant channels for ion adsorption-desorption which enhances its performance as an electrode material. As biomass naturally possesses a fine structure, retaining it in activated carbon promotes electrolyte circulation and enhances the material's electrochemical performance [41].



Figure 10: Biomass derived activated carbon as supercapacitor electrode [42].

### 1.6.2 Challenges in Activated Carbon

The main factors affecting the performance of carbonaceous materials are pore size and surface area. In general, a larger surface area is beneficial for improving the capacity and overall performance of supercapacitors. However, the three-dimensional conductive network gets broken with increase in surface area after a certain value, reducing its electrochemical

performance as an electrode material [43]. Therefore, introducing another material in the 3D porous structure of activated carbon might help retain its structure and conductivity.

## **1.7 Research Objectives**

The following are the main objectives of this research:

- Designing material which could meet the challenges in the field of supercapacitors.
- Synthesis of MXene and biomass derived activated carbon
- Synthesis of MXene/activated carbon composite.
- Characterization of the materials using XRD, SEM, Raman and BET.
- Electrochemical characterization by CV, GCD, EIS and cyclic stability.



## CHAPTER 2: LITERATURE REVIEW

### 2.1 Supercapacitors for Energy Storage

The most important energy conversion and storage technology in modern sustainable and renewable nanotechnology is the supercapacitor. Supercapacitors are revolutionizing advanced energy applications with their huge energy capacity, quick energy supply, and extended lifespan. Supercapacitors can be used effectively at high power levels to increase the efficiency of energy storage technologies. It has attracted considerable attention due to its high performance and long cycle life (>100 times battery life), which offers excellent opportunities for the development of more complex hybrid energy systems for stationary and vehicle applications [44]. SCs could eventually be used to replace or supplement batteries in energy storage (continuous power supply, load balancing). Due to their unique structure and internal storage mechanism, supercapacitors can be divided into three main forms: hybrid supercapacitors, pseudo-capacitors and electric double layer capacitors (EDLC). An EDLC is formed by connecting two parallel wires between dielectric layers as electrodes and supplying voltage to one side and grounding the other side. Charge accumulates on both sides of this structure until electrostatic equilibrium is reached [45]. A pseudocapacitive mechanism occurs when charges accumulate on both sides of the electrode and are quickly stored on the electrode surface through redox processes [45]. Hybrid supercapacitors combine the advantages of pseudocapacitors and double-layer capacitors and often have performance characteristics intermediate between these two types of capacitors [46]. Although electric double layer capacitors have high power density due to their highly reversible ability to accumulate charge on both sides, their energy density is relatively lower than that of batteries. Pseudocapacitors have a large contact area, short electron transfer path length, short ion diffusion length and even longer cycle life and are energy storage devices that work in conjunction with EDLC through the Faraday redox process [47]. However, if the shape, structure, composition, structure and properties of the electrode membrane are not well controlled, there is a risk of reducing the electroactive surface area, adsorption sites and performance. Non-Faraday surface response on electrodes combined with Faradaic embedding in hybrid supercapacitors [48]. By constructing electrodes from 3D mesoporous structural materials, hybrid supercapacitors can maintain remarkable cycling stability and be economical at

high power and energy density despite the limited conductivity of some types of carbon and metal oxide-based electrodes [49].

## **2.2 Conventional Electrode Material**

The choice of material for the supercapacitor electrode is important since it has an impact on the electrical characteristics [6]. New electrode materials for supercapacitors should have strong conductivity, good surface function, high specific surface area, pore size adjustability, electrolyte solution permeability and electrode wettability to improve capacity [50]. For supercapacitors, electrode materials with high energy storage and high electron collection ability should be developed. The researchers examined metal oxides and hydroxides as well as carbon compounds and conductive polymers as possible options for electrode materials.

### *2.2.1 Carbon based Materials*

Commonly used electrode materials in supercapacitor construction are various forms of carbon compounds. Reasons for this include the large surface area, accessibility, affordability and proven electrode manufacturing technology. The electrochemical double layer formed at the interface between the electrode and electrolyte acts as a storage mechanism for the carbon material [6]. Therefore, the surface area that the electrolyte ions can reach primarily determines the capacity. Specific surface area, surface functionality, shape, pore structure, pore size distribution and conductivity are important determinants of electrochemical performance [51]. For carbon materials, the large surface area facilitates higher charge accumulation at the electrode-electrolyte interface. In addition to pore size and high specific surface area, surface functionalization is an important factor that must be considered when increasing specific capacity.

Carbon nanotube electrodes arise due to their properties such as excellent electrical conductivity, thermal and chemical stability, low mass density, special mesoporous internal network and accessible external structure with large surface area [52]. Single-walled carbon nanotubes (SWCNTs) and multi-walled carbon nanotubes (MWCNTs) are two types of carbon nanotubes (CNTs) that are often investigated for supercapacitor electrode material. Compared to activated carbon, CNTs have a lower surface area ( $<500 \text{ m}^2/\text{g}$ ), leading to a reduced energy density [53].

Q. Cheng et al.[52] studied the electrochemical properties of graphene, carbon nanotubes (CNTs), and their solar cell (SC) composites in a series of electrolytes. In ionic liquids, the graphene/carbon nanotube electrode exhibits enhanced electrochemical properties, including a 263.2 kW/kg power density and 155.6 Wh/kg energy density, as well as a specific capacitance of 290.4 F/g.

Xie et al.[54] used willow catkins and the straightforward carbonization and KOH activation procedure to create hierarchical porous carbon microtubes (HPNCTs). The finished product had a highly porous structure as the result of the activation procedure and a tubular structure that was obtained from the willow catkins. The final product had a specific surface area of 1775.7 m<sup>2</sup>/g and a gravimetric capacitance of 292 F/g.

### *2.2.2 Metal Oxide based Electrode Materials*

Metal oxides are another option for supercapacitor electrode material since they have a high specific capacitance and low value of resistance, making it easier to build supercapacitors with high energy and performance [55]. Due to the reversible redox process on the surface of metal oxides, they have a greater ability to store energy, resulting in high capacity: ruthenium dioxide (RuO<sub>2</sub>), nickel oxide (NiO), iridium oxide (IrO<sub>2</sub>) and manganese oxide (MnO<sub>2</sub>). are the most used metal oxides. They are a viable substitute due to their gentler electrolyte and reduced production costs.

Transition metal oxides (TMOs) (FeO, V<sub>2</sub>O<sub>5</sub>, RuO<sub>2</sub>, TiO<sub>2</sub>, Nb<sub>2</sub>O<sub>5</sub>, SnO<sub>2</sub> and Co<sub>2</sub>O<sub>3</sub>) are a desirable contender for supercapacitor applications because of their numerous oxidation states. Transition metal oxides have greater energy storage capability than carbon electrodes, making supercapacitors more attractive than theory predicts because of their low electrical conductivity and small surface area. However, because of low conductivity and insufficient surface area, metal oxides have a lower capacity than theoretically predicted [56].

Ruthenium Oxide, have properties, including high metallic conductivity, chemical and thermal stability, and field emission behavior, all these properties make RuO<sub>2</sub> (either crystalline or amorphous) crucial for theoretical and practical applications. RuO<sub>2</sub> has become the most

successful material attributable to its high specific capacity, reversible redox reaction, wide potential window and long cycle life [57].

RuO<sub>2</sub> is produced electrochemically through an electrodeposition process and used in supercapacitors. The resulting electrode produced a specific capacitance of 498 F/g at a scan rate of 5 mV/s and remained stable over a long period of time [58].

Kong S. et al.[59] fabricated the RuO<sub>2</sub>-GC electrode using GNSs and CNTs placed onto CNFs. RuO<sub>2</sub> and carbon-based material together produced a specific capacitance of 480.3 F/g at 0.6 A/g. Also, it showed a 30.9 Wh/Kg energy density and a 1400 W/Kg power density.

Nickel oxide is an attractive electrode material for supercapacitors due to its low cost, rapid production, and environmental friendliness. Electrochemical methods are characterized by simplicity, economy, accuracy, adaptability and reliability. Nickel hydroxide is converted into nickel oxide using electrochemical technology. With the resulting method, a 1478 F/g specific capacitance was obtained in 1 M aqueous KOH electrolyte [60].

S. Goel et al.[61] produced NiO nanoflakes using the microwave-assisted approach, the results showed that the material had excellent pseudocapacitive performance when used as supercapacitor electrode material. They also showed a surface area of 206 m<sup>2</sup>/g and a high conductivity of 33.87 S/cm at ambient temperature.

M. Aghazadeh et al.[62] used electrochemical methods to convert nickel hydroxide into NiO. The NiO electrode used in this method showed 91.8% capacity retention after 3000 cycles at a scan rate of 5 mV/s and a specific capacitance of 1541 F/g in 1 M KOH.

### *2.2.3 Conducting Polymer Based Electrode Materials*

Extensive studies on many conductive polymers as electrode materials for supercapacitor have been done due to their low cost and ease of preparation [63]. Conducting polymers electrode materials, they exhibit higher conductivity, comparable series resistance to carbon-based electrodes and high capacitance. Since there are no structural changes, like as phase transitions, during the charge/discharge mechanism, conducting polymers can hold the charge in its bulk. Conductive polymers can offer higher capacity due to their larger surface area

and redox storage ability. The specific capacitance in conducting polymers arises from fast reversible redox reactions induced by  $\pi$ -conjugated polymer chains. During these reactions, ions migrate to the polymer framework through an oxidation process (also called doping) and are then released into the electrolyte during a reduction process (also called dedoping) [56]. Despite these advantages, the mechanical stress caused by reduction and oxidation in conducting polymers limits stability and degradation during multiple charge-discharge cycles. Another disadvantage of conducting polymers that affects their effectiveness is their low power density, which is due to slow total ion diffusion rates.

PANI, due to its affordability, excellent energy storage capacity, high electrical conductivity, and ease of synthesis, polyaniline is regarded among the best performing supercapacitor electrode materials among several conductive polymer types. However, the properties of polyaniline deteriorate rapidly due to repeated expansion and contraction (charge/discharge) cycles. Combining polyaniline with carbon materials has been shown to increase the capacitance value and improve the stability of PANI to overcome this limitation [56].

Wang et al.'s [63] electrochemical polymerization process was used to create PANI, which served as the supercapacitor's active ingredient. At 1 A/g, it offered a specific capacitance value of 950 F/g. It was reported that at high current densities the high specific is made possible by the array's unique nanowire structure, which reduces diffusion routes and charge transfer resistance.

Fabrication of energy storage devices requires high-performance electrode materials found in conductive polymer hydrogels with mechanical flexibility and structural control that can alter electrochemical properties. PPY has good flexibility and higher conductivity than other conductive polymers. It can withstand rapid redox reactions for charge storage and has conductivities of 10 to 500 S/cm [64].

Y. Shi et al.[65] synthesized a conductive polypyrrole hydrogel nanostructure through the use of an interfacial polymerization approach, which yielded a 3D porous PPy network with 380 F/g specific capacitance.

### **2.3 2D Material as Electrode Material for Supercapacitors**

Since the astonishing discovery of “exfoliated” single-crystalline graphite films in 2004, scientists have been very interested in two-dimensional materials with layered structures because of their amazing capabilities [66]. Through various preparation and exfoliation techniques, a variety of two-dimensional nanomaterials were obtained from various layered precursor materials, including transition metal dichalcogenides (TMD), hexagonal boron nitride (hBN), metal-organic frameworks (MOF), layered double hydroxide (LDH), black phosphorus (BP), metal nitride (MN), graphitic carbon nitride (g-C<sub>3</sub>N<sub>4</sub>), TMO and various MAX phases (such as Ti<sub>2</sub>AlC) used to derive 2D transition metal carbides, carbonitrides and nitrides (also known as MXenes) [67].

### 2.3.1 Graphene

It is a monatomic thick 2D structure which has been recognized as an emerging carbon material which can be used in energy storage application because of its properties, including high surface area, high electrical conductivity and chemical stability [68]. It has recently been suggested as an electrode material for supercapacitor applications because, unlike other carbonaceous materials such as CNTs, graphene does not depend on the solid-state pore distribution [69].

C. Liu et al.[68] obtained single layer graphene by the preparation curved graphene sheets. This prevented the restacking. Electrochemical results showed energy density of 85.6 Wh/kg at ambient temperature and energy density of 136 Wh/kg at 80 °C at a current density of 1 A/g. The obtained energy densities are comparable to those of the nickel metal hydride battery.

### 2.3.2 Transition metal dichalcogenides (TMDs)

Transition metal dichalcogenides (TMD) are layered compounds with the crystal structural formula MX<sub>2</sub>, where X is any element of chalcogenides like S, Te or Se and M can be any element of transition metals such as V, Re, Mo, Ta, Ti or W. Van der Waals forces hold the TMD monolayers together. Each layer consists of three atomic layers, between the two chalcogen layers lies a layer of transition metal [70]. In comparison with graphene, many two-dimensional TMDs are semiconductors. TMDs like MoS<sub>2</sub>, NbSe<sub>2</sub> and TiS<sub>2</sub> have a layered structure resembling graphite and are the first descendants of graphene. Their flexible, thin, and

transparent structures are nearly identical to those of graphene. Due to their exceptional physicochemical qualities, which include high chemical stability, good semiconducting ability, large surface area, high mechanical properties, ease of synthesis through a variety of preparation techniques and low cost. TMDs have generated a great deal of interest as electrode materials [67].

Y. Zheng et al.[71] developed a hybrid supercapacitor using a single-step hydrothermal process. Electrochemical supercapacitor performance of VSe<sub>2</sub>/RGO hybrid materials has been documented with a specific capacitance of 680 F/g at 1 A/g current. It has a high energy density of approx. 212 Wh/kg with approx. 3.3 kW/kg power density. Furthermore, capacity retention was 81% after 10,000 cycles.

### *2.3.3 Metal-organic frameworks (MOFs)*

Hybrid materials, or MOFs, possess a crystal structure and high porosity. They consist of organic and inorganic components held together by covalent coordination bonds. Since their first invention by Yaghi et al [72] in 1995, MOFs have gained wide attention because of their versatility, easy processing, low production cost, tunable structure and improved electrochemical response. These materials store charge through their pseudocapacitive properties. In addition to the many excellent electrochemical properties of MOFs, their high crystallinity also brings with it some significant disadvantages, such as at higher charge/discharge rates they show short cycle stability and reduced conductivity [73].

Zhen He et al.[74] created a composite of MnO<sub>2</sub>/carbon nanosheets for electrode material for SCs. The Mn-based MOF nanosheets were carbonized and MnO<sub>2</sub> nanosheets were vertically aligned using a straightforward low-temperature oxidation of MnO. In 1M Na<sub>2</sub>SO<sub>4</sub> electrolyte, the as-synthesized MnO<sub>2</sub>/CNS demonstrated 339 F/g specific capacitance value at 0.5 A/g.

## **2.4 MXene: Structure and Composition**

In 2011, Yury Gogotsi created the MXenes material, which is a component of the MAX phase, a class of two-dimensional inorganic substances [75]. The MAX phase is a class of materials with the general formula M<sub>n+1</sub>AX<sub>n</sub>, where M is an element from Group IIIA or IVA of the periodic table (e.g. elements from Groups 13-16 such as In, Ga, Al, As, Ge), Pb and Sn) A is from group

IIIA or IVA, X is carbon or nitrogen [76]. There are different categories of MAX phases based on the value of “n” (e.g. 413, 211, 514, 312, etc.). The M-A bond is metallic in nature while the M-X bond is metallic, ionic or covalent in nature. Using a slightly weaker M-A metal compound, a chemical etch layer can be performed to produce MXene. MXene has the formula  $M_{n+1}AX_nT_x$  ( $n= 1-3$ ), where  $T_x$  represents the termination groups of surfaces (such as -OH, -Cl, -O, -F etc) [77].

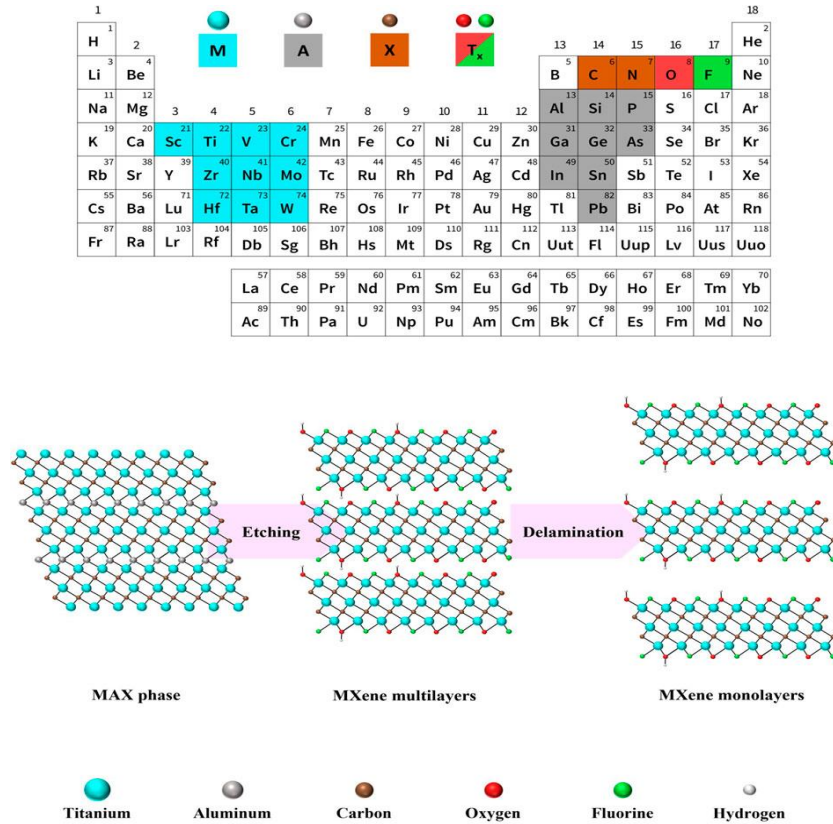


Figure 11: MAX phase to MXene [78].

There are different methods to synthesize MXene some of them are discussed below.

#### 2.4.1 HF Etching

Different source materials, compositions, sintering and processing conditions have all been used to make MXenes. For the required stoichiometric ratio Ti:Al:C,  $Ti_3AlC_2$  can be formed if suitable sintering conditions are met. Subsequent properties of  $Ti_3C_2T_x$  such as surface finish, flake consistency and size (for example, the type of defects and number of defects) relate



directly to the method of preparation. Most synthesis techniques described in previous studies involve HF of 10 to 50 wt%, although less HF is required to extract aluminum from  $\text{Ti}_3\text{AlC}_2$ .

It is worth noting that when selectively etching aluminum, smaller HF concentrations (5 wt% HF, about 24 hours) produced results comparable to higher concentrations (10 wt% HF, 18 hours and 30 wt% HF, 18 hours) were quite comparable. According to most MXene literature, concentrated HF is the recommended etchant for Al extraction from  $\text{Ti}_3\text{AlC}_2$ . Yet, the utilization of highly concentrated HF may be eliminated if the etchant is diluted using HF of 5% concentration. MXene produced by HF etching has an accordion-like shape that holds the 2D layers together through hydrogen bonds and van der Waals forces. If diluted HF (<6 M) is used, the structure of MXene appears as broader layers with limited gaps between stacks, indicating a reduced separation of the MXene layers. On the other hand, etching MXene with lower HF concentrations helps  $\text{H}_2\text{O}$  molecules move between layers and creates more exposed interlayer gaps, which provides more active sites for ions to reach as well as increases the capacity. Furthermore, MXenes with reduced defect levels are caused by the softer etching conditions [75].

#### *2.4.2 Alkali Etching*

Alkaline etching has also been recently investigated for the synthesis of MXene and produced MXene with excellent performance. MXene is sensitive to dissolved oxygen, so it is important to pass argon through deionized water to remove dissolved oxygen. Using hydrothermal treatment method followed by repeated cleaning with concentrated NaOH in degassed water the MAX phase can be etched effectively [79].

#### *2.4.3 Electrochemical Etching*

It has also been demonstrated that this procedure is an effective way to prepare MXenes. By employing HCl in low concentration as an electrolyte in the electrochemical etching of  $\text{Ti}_2\text{AlC}$ ,  $\text{Ti}_2\text{CT}_x$  can be generated. The process also extracts some titanium, causing carbide-generated carbon to deposit on the MXene surface. This process resulted in the  $\text{Ti}_2\text{CT}_x$  displaying -O, -OH and -Cl functional groups rather than -F ended functional groups. Additionally, a method for synthesizing other MXenes, such as  $\text{Ti}_2\text{CT}_x$ ,  $\text{Cr}_2\text{CT}_x$ , and  $\text{V}_2\text{CT}_x$ , has

been devised that uses electrochemical thermal assistance, where the kinetics of etching is enhanced by gentle heating environment of around 50 °C. MXenes produced with this method have particles with 25 nm lateral size and a flower-like morphology [80].

## 2.5 MXene as Electrode for Supercapacitors

MXenes' unique blend of metallic conductivity and hydrophilicity makes them an appealing choice for energy storage, particularly as electrodes for supercapacitor applications. When compared to traditional carbonaceous materials, MXene has demonstrated its ability to function as an ultra-high volumetric supercapacitor. These unique qualities, such as its high electric conductivity, large densities, hydrophilicity and faradic pseudocapacitive nature, may be the cause of this. Therefore, MXene can be used as a current collector to move electrons and as an active material for electrodes to store charges. Due to these properties, additional dense current collectors are not required and MXenes supercapacitors with large surface and volume capacitances can be constructed to produce smart electronic devices [31].

Zhang et al.[74] created a conductive, free-standing, highly deformable electrode by combining MXene and MnO<sub>2</sub> in a composite on carbon fabric. The resulting electrode was compared beside MnO<sub>2</sub> nanorods/CC electrode (with a specific capacitance of 302.3 F/g). An improved specific capacity of about 511.2 F/g was observed.

Jing Guo et al.[81] synthesized a d-Ti<sub>3</sub>C<sub>2</sub>/NF composite via self-assembly method of electrostatic attraction of positive and negative charges. The positive electrode material displayed an excellent electrochemical performance with a specific capacitance of 654F/g at current density of 1 A/g, as well as good cycling stability. The findings stem from the direct contact between Ni- foam and d-Ti<sub>3</sub>C<sub>2</sub> nanosheets, as well as the high conductivity of the nanosheets, which produces a high specific capacitance and facilitates quick electron transfer. Maximum power density and energy density are delivered by d-Ti<sub>3</sub>C<sub>2</sub>/NF//b-Ti<sub>3</sub>C<sub>2</sub> asymmetric supercapacitor with 4731.4 W/kg (9.2 Wh/kg) and 18.1 Wh kg<sup>-1</sup> (397.8 W/kg). Furthermore, the asymmetric supercapacitor has excellent stability (80.6% after 5000 cycles).

Chunyuan Zhu et al.[82] prepared Co(OH)<sub>2</sub>-Ti<sub>3</sub>C<sub>2</sub>T<sub>x</sub>@NF by coupling MXene nanosheets and cobalt hydroxide. Nickel foam as a conductive substrate provides a cross-linked framework for

rapid electrolyte diffusion, and the formation of the heterostructure successfully suppresses the self-agglomeration of MXene and cobalt hydroxide. The results showed a specific capacity of up to 1400 F/g. A 98.2% cycle stability after 10,000 cycles was also achieved. The asymmetric supercapacitor has an energy density of  $13.7 \mu\text{Wh}/\text{cm}^2$  @NF//AC at  $1.4 \text{ mW}/\text{cm}^2$ .

Liyong Zhang et al.[83] successfully prepared a self-supporting  $\text{Ti}_3\text{C}_2\text{T}_x$  /NF electrode structure through high electrostatic fields using monolayer  $\text{Ti}_3\text{C}_2\text{T}_x$  MXene ink. outstanding supercapacitor performance might be achieved by efficiently suppressing the aggregation of monolayer  $\text{Ti}_3\text{C}_2\text{T}_x$  MXene, as demonstrated by a high specific capacitance of  $319 \text{ mF}/\text{cm}^2$  at  $2 \text{ mA}/\text{cm}^2$  and 94.4% cycling stability after 7000 cycles.

## 2.6 Biomass derived Carbonaceous Materials

A carbon-rich material known as biomass-derived carbon is created when biomass is heated to a high temperature and is oxygen-free. The material has a high carbon content, excellent electrical conductivity, large specific surface area and good stability, making it useful in research areas including wastewater treatment, power generation and energy storage [84]. In contrast to conventional electrode materials, carbon materials obtained from biomass are inexpensive, readily available, and environmentally benign. Furthermore, by adding additional heteroatoms, their special porous structure can enhance their electrochemical performance or make it easier for ions to move throughout the electrolyte. Some of the biomass derived carbonaceous materials are:

- CNFs
- CNTs
- Graphene
- Activated Carbon

### 2.6.1 Precursors for Biomass derived Carbonaceous Materials

The most important factor in producing carbonaceous material derived from biomass is using simple techniques, raw material that is easily available and cheap. Biomass is typically carbohydrate composites that come from human excretions, plants and animals. Their main component is carbon, but some also contain heteroatoms such as oxygen, sulfur and nitrogen

[85]. In addition to reducing production costs and converting waste into valuable materials, the conversion of biomass to materials that is usable can partially solve the problem of environmental pollution. After extensive research scientists have found a wide range of precursors that can be used for biomass-derived carbon synthesis. Biomass precursors are mainly divided into four types [84]:

- Biomass from plants: The most often utilized carbon precursor components generated from biomass are hemicellulose (20–40 wt%), cellulose (40–50 wt%) and lignin (10–40 wt%), which make up most plants.
- Biomass from animals: The composition of these precursors is more complex compared to plant precursors. To date, animal protein and chitosan have commonly been used for biomass carbon production.
- Biomass from humans: Due to the economy's rapid growth, human civilization produces a large amount of industrial and home garbage every day that is challenging to recycle. Right now, domestic trash produced by people is growing at a quick rate, and urbanization is happening faster in every country in the world. In addition to requiring the occupation of land, the dumping of these household wastes pollutes the environment and has an adverse effect on human health. Because of their high carbon content, plastics, leftovers, leather, textiles and abandoned wood, among other household wastes, can be used to derive carbonaceous material.
- Biomass from microorganisms: Microorganisms are carbonaceous organisms that reproduce rapidly, are widespread and diverse. Commonly used in the food and pharmaceutical industries, it contains bacteria, actinomycetes, fungi, viruses and other tiny prokaryotes. Since peptidoglycans form the cells of most microorganisms, they can be used as precursors for carbon produced from biomass.

There are different methods for the synthesis of carbonaceous materials from biomass, some of them are discussed below.

### *2.6.2 Pyrolysis*

The most popular thermochemical process for producing carbon materials derived from biomass is pyrolysis. Biomass precursors undergo various conversion reactions at high

temperatures (300–1000 °C) in inert gas, ammonia or oxygen-poor atmospheres. The end product is mainly carbon from biomass, liquid bio-oil and volatile materials (CO<sub>2</sub>, CH<sub>4</sub> and other organics). These reactions typically include dehydration of the biomass, then condensation, after that formation of network, occurrence of depolymerization, cracking and finally isomerization. This is advantageous because of low pollution, simple process, low cost and production at large-scale, but resulting product has poor pore structure, low specific surface area and many impurities [86].

### *2.6.3 Hydrothermal Carbonization*

The hydrothermal method, which combines simplicity, energy efficiency, and environmental protection, is an efficient way to manufacture carbon extracted from biomass. The biomass precursor will go through thermochemical transformation with water medium inside a closed system during the hydrothermal reaction process at relatively low temperatures in the range of 100 to 300 °C, ultimately yielding the carbonaceous material derived from biomass. Specifically, critical or supercritical water can provide autonomous pressure in the reaction system in addition to increasing the reactivity of biomass precursors. After the hydrothermal reaction, there are still many oxygen-containing functional groups (COOH, OH and C=O) on the surface of the carbon produced from biomass. This has significant advantages for the additional functionalization of carbon obtained from biomass, which can expand the range of applications. However, the carbonaceous material produced from this method has small specific surface area, poor porosity and low electrical conductivity; therefore, it is required to get greater activation before using it as supercapacitor electrode material [87].

### *2.6.4 Activation*

Hydrothermal carbonization method and pyrolysis don't give satisfactory results when it comes to porosity and surface area. To resolve this issue, scientists have found activation processes. Depending on the process, activation methods are classified into physical or chemical activation methods [84].

Physical activation involves heating biomass precursors to a specific temperature to produce biomass char. The biochar is then activated with oxidizing gases (CO<sub>2</sub>, N<sub>2</sub>, water vapor, air) at

temperatures above 800 °C, which ultimately creates carbon derived from biomass [38]. The physical activation approach features low instrument loss, high yield, and a straightforward process when compared to alternative preparation methods. Additionally, there is no need for additional processing because the products made using this approach can be used right away. However, to use this process, a greater reaction temperature is needed, which will use more energy and result in more pollutants.

Chemical activation necessitates a lower temperature, short reaction time as well as a more perfect porosity structure in the result than physical activation. During chemical activation, biomass precursors are combined with activation reagents and heated to temperatures between 300 and 950 °C. This can simultaneously complete carbonization of the product as well as activation. Many activation reagents, including NaOH, KOH, ZnCl<sub>2</sub>, FeCl<sub>3</sub>, H<sub>2</sub>SO<sub>4</sub>, H<sub>3</sub>PO<sub>4</sub>, and Na<sub>2</sub>CO<sub>3</sub>, have been developed to date [88]. KOH is the most commonly used activator. The carbon element reacts with KOH, K<sub>2</sub>O and K<sub>2</sub>CO<sub>3</sub> formed during the pyrolysis process, etching the matrix of carbon and developing a porous structure. Moreover, the pyrolysis process produces CO, H<sub>2</sub>, CO<sub>2</sub> and H<sub>2</sub>O which create additional pores in the end product [89]. Moreover, a loose carbon structure will arise from the pyrolysis reaction's intermediate product, metallic K, entering the carbon lattice. Eventually, after being thoroughly cleaned with water, the carbon generated from biomass can be recovered. This activation method improves the specific capacity and porous structure of biomass-derived carbonaceous materials and reduces energy loss during the manufacturing process.

## **2.7 Activated Carbon as Electrode Material for Supercapacitor**

As an electrode material for supercapacitors, activated carbon (AC) has attracted much attention due to its advantages such as high specific surface area, large porosity, high electrical conductivity, high adsorption capacity and low cost. It can be synthesized from a range of biomass precursors such as wood, peanut shells, apple peels, banana peels, wheat husks, etc. Large electrochemically active surface areas, quick ion transfer kinetics, and high electron conductivity are all results of the linked porous structures found in AC, which makes AC a promising electrode material [42].

Su et al.[90] used KOH chemical activation to create SAC (activated carbon) produced from loofah sponges. They discovered that adjusting the concentration of KOH could efficiently control the HPC (hierarchical pore structure) of SAC. Consequently, the resulting SAC displays a high heteroatom functional groups concentration (19.2 at%) and 2718 m<sup>2</sup>/g surface area, which contributes to 16.1 Wh/kg energy density in the Na<sub>2</sub>SO<sub>4</sub> electrolytes showing a superior performance.

Deng et al.[91] attained a 253 F/g specific capacity using HPC material. HPC is synthesized in a one-pot process, carbonized at 900°C and treated with KHCO<sub>3</sub>.

Gou et al.[92] achieved a specific capacitance of 226.2 F/g at current density of 0.5 A/g with HPC material. It was synthesized by carbonizing wheat straw at 400 °C and KOH activation.

M. M. Baig et al.[93] used activated carbon and achieved a specific capacity of 271.5 F/g at a current density of 0.5 A/g, with a capacity retention of 82% after 5000 cycles. It is synthesized by carbonizing wheat husks at 400 °C in an N<sub>2</sub> environment and activating them at 800 °C.

## CHAPTER 3: MATERIALS AND METHODS

### 3.1 Materials

MAX phase ( $\text{Ti}_3\text{AlC}_2$ ) was purchased from Sigma Aldrich (CAS-No: 196506-01-1). HF, HCl, ethanol and DMSO were purchased from Sigma Aldrich.  $\text{HNO}_3$  was purchased from Fisher. KOH was purchased from Daejung chemicals (CAS-No.: 1310-58-3). DI water was purchased from HAT Enterprises Pakistan. All materials and chemicals were of analytical grade. Barley was purchased from a local market which was used in the synthesis of activated carbon.

### 3.2 Synthesis of MXene ( $\text{Ti}_3\text{C}_2\text{T}_x$ )

Multilayered MXene was synthesized by selective etching method [94]. 20 mL of HF was added to the Teflon container, then slowly 1 g of MAX phase was added to the acid, placed in an oil bath at a temperature of 50 °C and the mixture was stirred for 24 hours. The mixture was then diluted with deionized water and the pH was maintained at approximately 7 by centrifugation five to six times at 4500 rpm (6 minutes per round). The etched sample was then dried at 60 °C overnight. For intercalation, 45 ml of DMSO were added to the MXene precipitate and stirred at room temperature and 300 rpm for 20 h. MXene sheets were then probe sonicated for 4 hours at 90% power of 650 Watt. For exfoliation of MXene sheets, the sample was then centrifuged once for 10–15 minutes at 3500 rpm. The sample was then dried overnight at 60 °C.

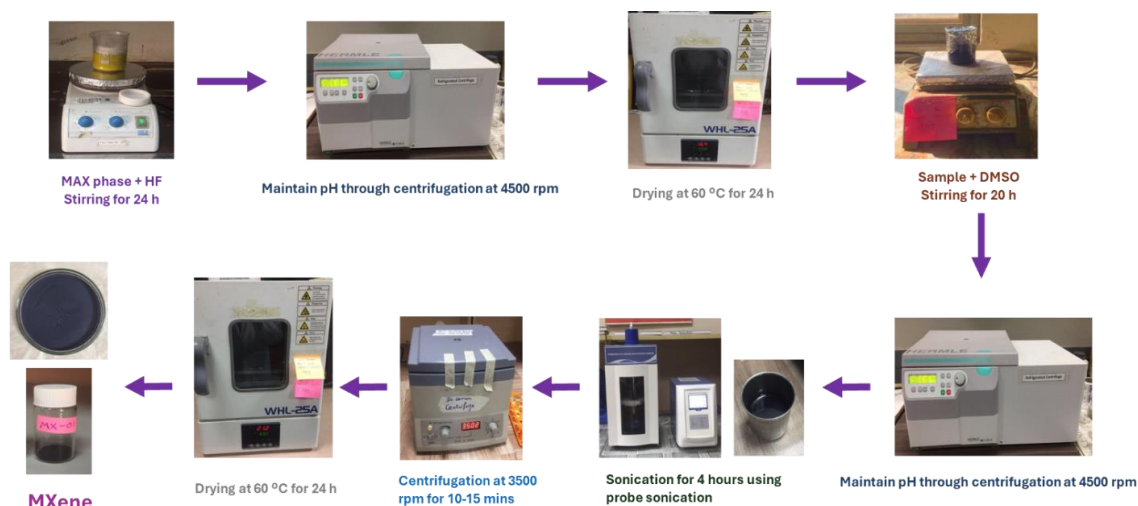




Figure 12: Synthesis process of MXene.

### 3.3 Synthesis of Activated Carbon

Activated Carbon was prepared using barley as precursor. For pretreatment, 25g of barley flour was added in 1M HNO<sub>3</sub> solution and stirred at room temperature for 24 hours. Afterwards, it was centrifuged at 4500 rpm for 6-7 times (7 minutes round) until the pH of sample reached approximately 7. The pretreated sample was dried overnight at 60 °C. The sample was then ground using mortar pestle to obtain powder. For carbonization, the powder was placed in an alumina crucible at 400 °C in a tube furnace and heated for 1 hour under a stream of nitrogen at a heating rate of 5 °C/min. To obtain a fine powder, biochar is ground in ethanol in a ball mill for 3-4 hours. The biochar was then dried overnight at 60 °C. For activation, biochar was mixed with KOH in a stoichiometric ratio of 1:5 and stirred in 30 ml of deionized water for 5 hours and 30 minutes. The sample was then dried overnight at 60 °C. Finally, the mixed powder was transferred to an alumina crucible and annealed in a tube furnace at 700 °C for 1 hour at a heating rate of 5 °C/min under a nitrogen atmosphere. The resulting product was washed by centrifugation (cycle 6 min) at 4500 rpm using 1 M HCl and deionized water until the pH of the sample was neutralized. The activated carbon sample was then dried at 60 °C for 24 h.

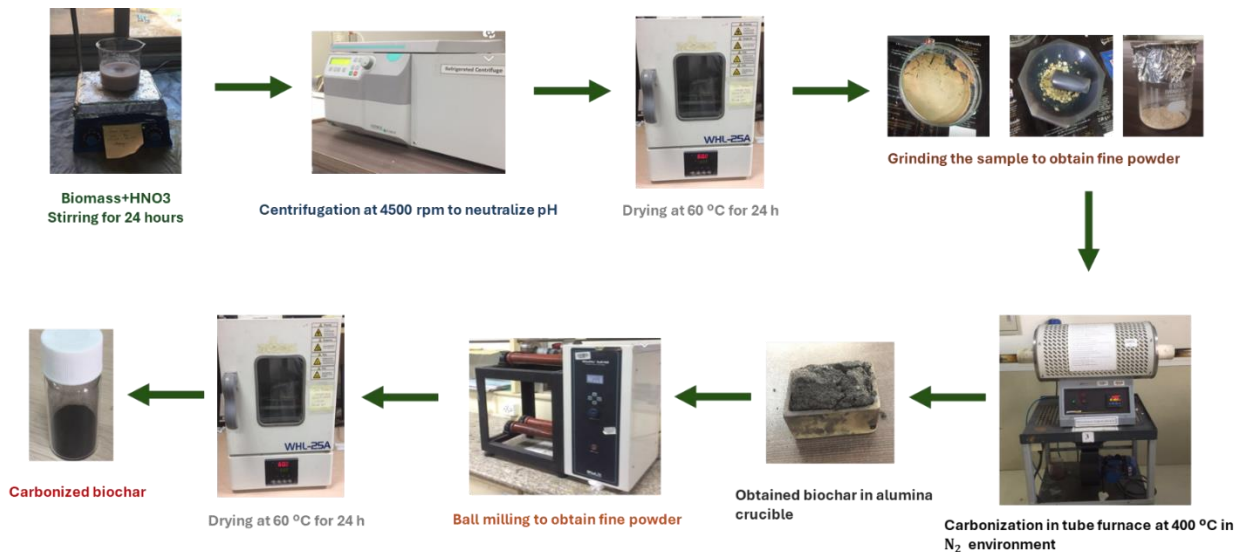
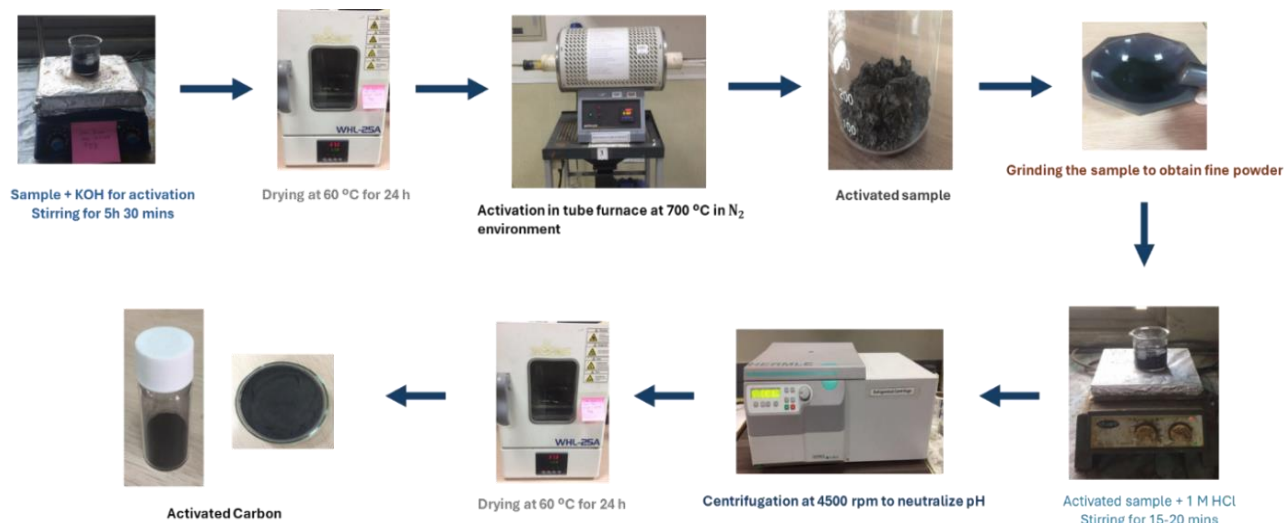


Figure 13: Synthesis of biomass derived activated carbon. (a): Carbonization Process.



(b): Activation process.

### 3.4 Synthesis of MXene/Activated Carbon Composite

For the preparation of MXene/Activated Carbon composites, AC was added in different wt%, 30%, 50% and 100% for MAC1, MAC2 and MAC3 respectively. Activated carbon and MXene were added to 30 ml of deionized water. The samples were then treated with ultrasound for 2–3 hours. The dispersions were vacuum filtered and then dried in a vacuum oven at 60 °C for 24 hours.

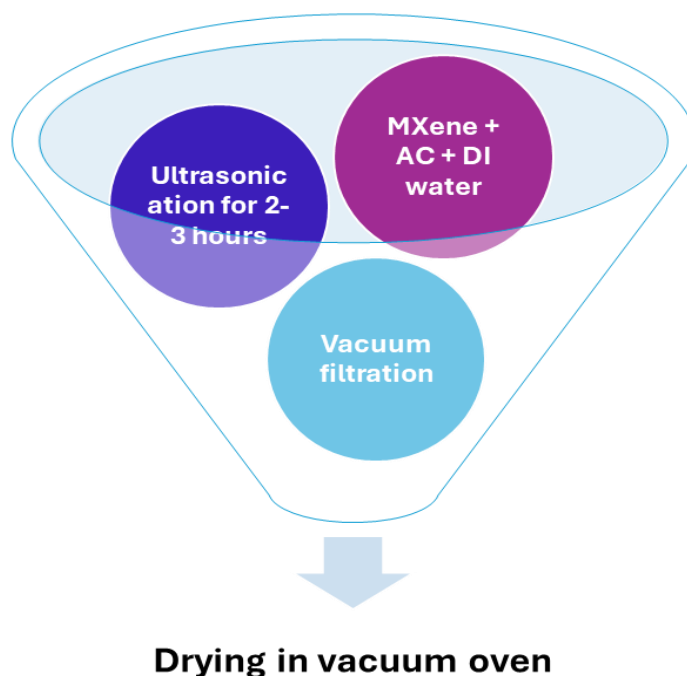


Figure 14: Synthesis process of MXene/AC composites.

### 3.5 Electrode Preparation

First, the nickel foam is processed into clean nickel foam. Cut it into 1cm x 1cm pieces, then added into a 1M HCl solution and ultrasonicated for 30 minutes. Then the solution was discarded, and the nickel foam pieces were sonicated in acetone for 30 minutes, then in ethanol, and finally in deionized water for 30 minutes. The nickel foam pieces were then dried overnight in a vacuum oven at 60 °C. For slurry preparation, MXene, activated carbon and their composites were used as active materials. The active material was mixed with carbon black as conducting agent, PVDF as binder and NMP as solvent in a weight ratio of 80%: 10%: 10% respectively. Then, the solutions were ultrasonicated for 1 hour to get a homogenous mixture. Each slurry was then dropped coated onto the nickel foam piece and dried overnight in a vacuum oven at 80 °C. To determine the mass loading of the sample, the nickel foam panels were weighed before and after coating.



Figure 15 : Electrode preparation process

## CHAPTER 4: CHARACTERIZATION

### 4.1 X-ray diffraction (XRD)

The working principle of X-ray diffraction analysis (XRD) is constructive interference between monochromatic X-rays and the crystalline sample [95]. This nondestructive technique is used to investigate the various crystalline phases present in the test sample. The wavelength of X-rays employed for analysis varies from 10 Å to 2.5 nm. It consists of five major components, sample holder, radiation source, radiation transducer, component to limit wavelength and signal processing. Most diffractometers have the X-ray source and detectors positioned on the same side of the sample, where the incident x-rays strike at an angle, reflect, and land on the detector. A filament in a cathode ray tube produces electrons when it is subjected to heat. Electrons are accelerated towards the target by applying an electric field. When an electric field is applied, electrons accelerate towards the target. When these electrons hit the target material's inner shells, characteristic X-rays are released. For X-ray diffraction, copper ( $\text{Cu-K}\alpha$  radiation = 1.5418 Å) is the most often employed target material. The goniometer is used to maintain the angle at which this monochromatic beam of X-ray is guided to fall down on the sample. The most widely used detector for measuring the intensity of X-rays reflected by constructive interference is the scintillation counter. Powder X-ray diffraction has a full scan range of 5° to 150°.

The layers and planes that make up a crystal cause the X-ray light to be dispersed when it strikes them. When the X-ray light's wavelength aligns with the crystal planes, it is reflected in a way that makes the angle of incidence equal to the reflection angle. The diffraction patterns are the result of interference, which depends on the distance between the surfaces.

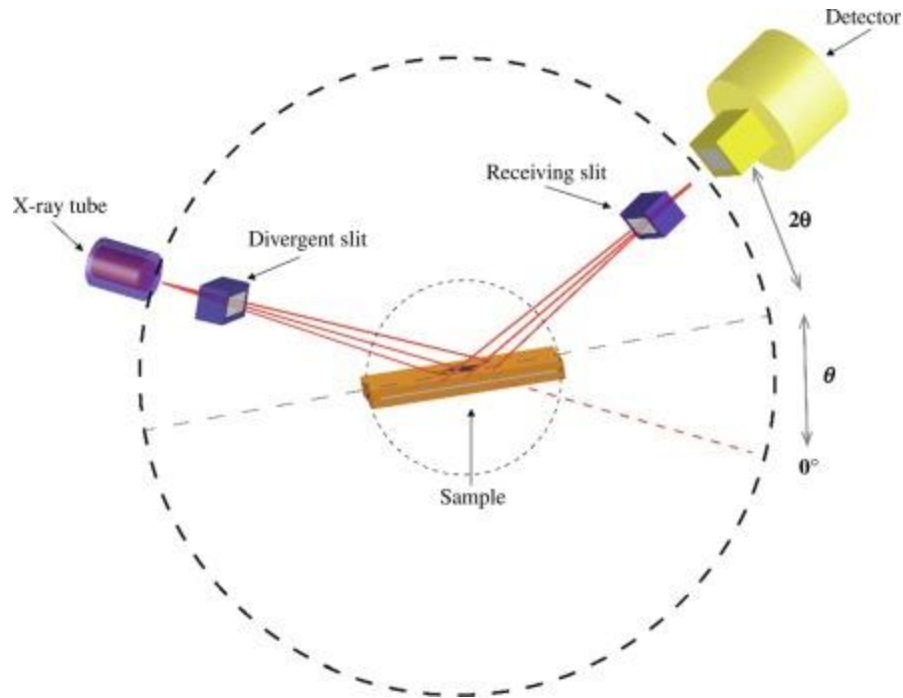


Figure 16: Mechanism of XRD [96].

W. H. and W. L. Bragg determined the correlation between the wavelength, d-spacing, and scattering angles of the X-rays in use in 1912. It is as follow

$$n\lambda = 2d\sin\theta$$

When Bragg's law is met, constructive interference occurs. This method provides information regarding a variety of sample characteristics, including, Sample purity, phase, crystallinity, lattice mismatch, dislocations and unit cell measurements.

## 4.2 Raman Spectroscopy

Raman spectroscopy's 0.5–1m spatial resolution makes it suitable for microscopic examination. With a Raman microscope, this kind of research is feasible. A Raman microscope uses a tiny laser focus to give Raman analysis and high magnification sample imaging. It is connected to a regular optical microscope via a Raman spectrometer. To undertake a Raman microanalysis, place the material under the microscope, focus, and measure. A genuine confocal Raman microscope may be used to study micron sized particles. Even the various layers of a multilayered sample (such as polymer coatings) and the properties and contaminants beneath the

surface of a transparent sample (such as fluid or gas inclusions in glass defects or minerals) can be examined with it. Raman spectral pictures, which are made up of hundreds of spectra of Raman recorded at various locations on the sample, can be created using motorized mapping stages. The distribution of chemical components as well as variations in other effects like stress/strain, crystallinity, polymorphism, and phase, can be seen using false color pictures based on the Raman spectrum [97].

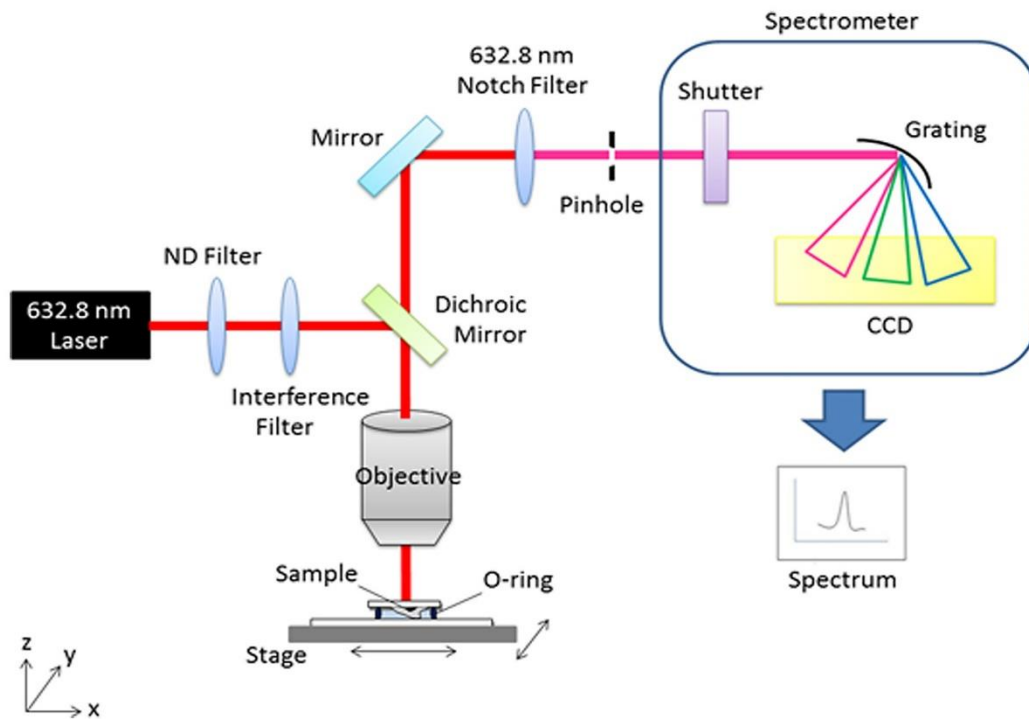


Figure 17: Working of Raman [98].

### 4.3 Scanning Electron Microscope (SEM)

SEM is a technique used for imaging, that visualizes bulk and nano surfaces using high intensity electron beams. When the extremely intense beam is directed on the sample surface, the information obtained includes, the sample's composition, sample topography and phase mapping [99].

Upon impact, the beam induces a variety of interactions that result in the emission of signals. These signals may include reversed scattered electrons, cathode luminescence, transmitted electrons, secondary electrons, and distinctive micro-X-rays.

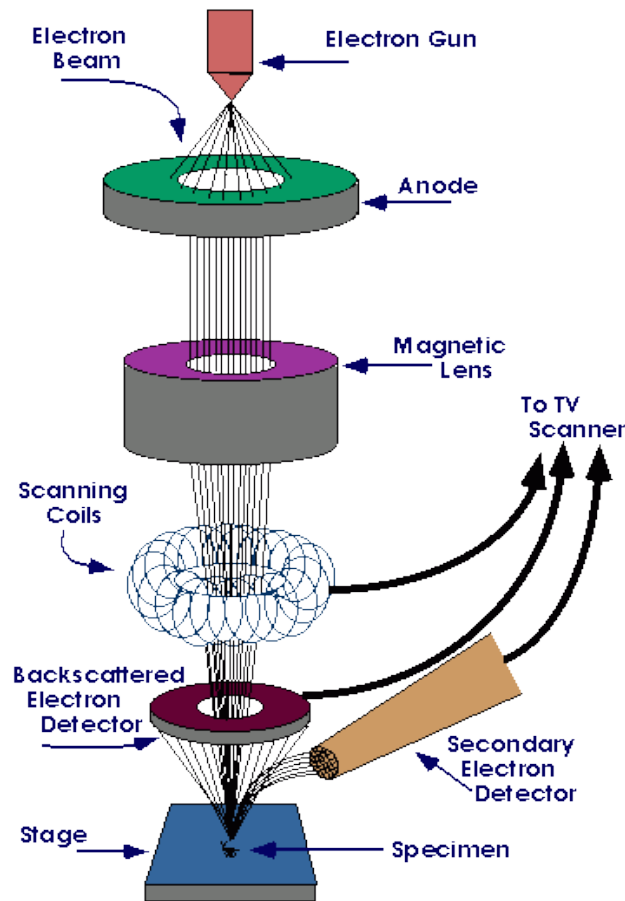


Figure 18: Working principle of SEM [100].

#### 4.3.1 Principle of SEM

In scanning electron microscopy, the sample surface is focused under the electron beam. The method utilized is a raster scan, which focuses on extremely small cross section areas. When the concentrated beam of electrons interacts with a material, the material's surface will release electrons or photons. Several sets of detectors are used to collect the released photons and electrons. The outputs from the detectors are used to control the cathode ray tube's brightness. The cathode ray tube (CRT) X and Y inputs are adjusted in accordance with the X and Y



voltages to restrain the electron beam. Consequently, image 1 was produced for a CRT display. Elemental x-rays, secondary electrons, and backscattered electrons all form images.

#### **4.4 BET Surface Area Analysis**

Through BET analysis, non-corrosive gases such as  $N_2$  are adsorbed or desorbed on the material's surface, allowing for the study of the material's porosity and surface area [101]. The sample is dried at a high temperature while  $N_2$  gas is being purged. The amount of  $N_2$  gas that has been adsorbed at the material's surface determines its porosity and surface area. An investigation on the volume of gas adsorbed on the surface is conducted using a continuous flow or volumetric procedure. The sample surface and  $N$  gas interact weakly with Van der Waal's forces when the temperature of liquid nitrogen is reached.

The BET multipoint measurement uses this equation. The mass of the material and the quantities  $V_m$  can be used to compute the specific pore surface area. Surface area and porosity, two crucial sample properties, are determined using the BET analysis approach. A sample preparation apparatus, an  $N_2$  transfer system, a sample tube, a vacuum pump, computer software and computer hardware make up the equipment. The sample is dried at high temperatures while non-corrosive gases like  $N_2$  are purged. The amount of gas adsorbed is then used to calculate the sample's pore size and specific surface area. One of the most important stages of the analysis is sample preparation. To remove all impurities, including water vapors as well as gas molecules, the sample is first purified by degassing in the sample preparation apparatus under vacuum conditions for a predetermined period. Following the placement of the sample test tube in the surface area, porosity analysis—which is related to the computing system and the quantity of adsorbing gases—was computed in relation to the total surface area and pore volume.

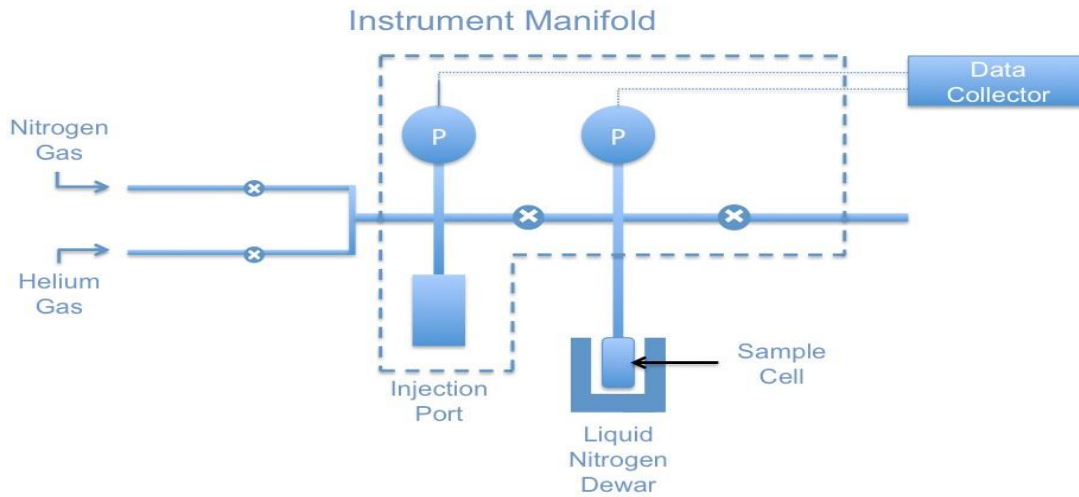


Figure 19: Mechanism of BET analysis [102].

#### 4.4.1 Sample Preparation for BET

First, degassing is done at a high temperature to remove various atmospheric pollutants from the sample, such as air, water vapor, etc. For degassing, vacuum conditions are necessary.

#### 4.4.2 Instrumentation of BET

The following components make up the instrumentation: Sample tube, reference container, temperature-controlled system from high temperature system to low temperature, monometer, gaseous pressure inlet, inert gas inlet, vacuum system.

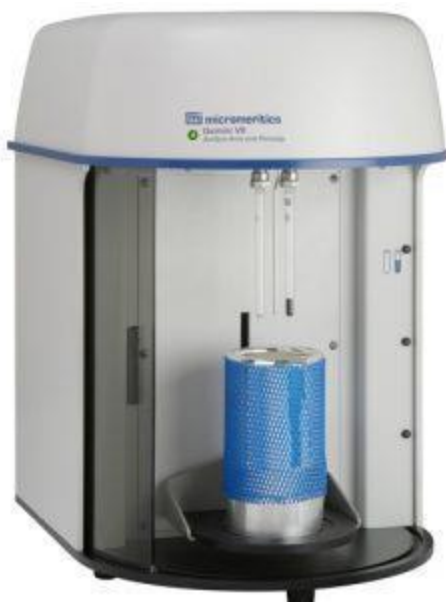


Figure 20: BET equipment [103].

## 4.5 Electrochemical Measurement

### 4.5.1 Cyclic Voltammetry

The most straightforward method for assessing electrochemical behavior at the laboratory scale is cyclic voltammetry (CV). The system comprises three electrodes: a reference electrode, a working electrode, and a counter electrode. The oxidation and reduction (redox) reactions at the electrode/electrolyte interface are then examined using the CV system. The plot of CV is between resulting current (I) of working electrode vs. potential (V) and is obtained when potential is applied to the working electrode and reference electrode, and the response of the output current between counter and working electrode is recorded. Platinum is typically employed as the counter electrode, and Ag/AgCl (silver/silver chloride) and SCE (saturated calomel electrode) are the most often utilized RE. The electrolyte's function is to supply ions, so it needs to have strong conductivity. In supercapacitors, different materials react differently. Whereas pseudocapacitors produce redox hump during forward and reverse scans, EDLC produces rectangular curves.

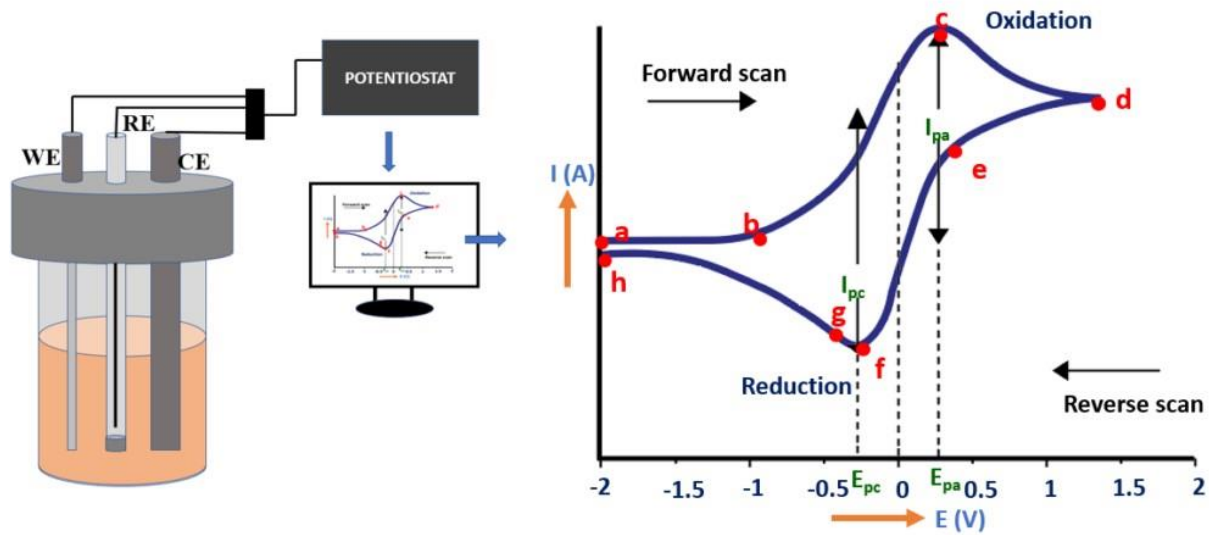


Figure 21: Three electrode based electrochemical cell set up and cyclic voltammogram [104].

#### 4.5.2 Galvanostatic Charge-Discharge Analysis

A popular technique for analyzing the charging/discharging characteristics of batteries and supercapacitors is GCD. Potential vs. time at constant current is measured by GCD. For a full cycle to be completed, the material needs to be once charged/discharged. The GCD curves of a pseudocapacitor and an EDLC diverge, just like in CV. During charge and discharge cycles, EDLC materials exhibit linear curves with minimal IR drop. The absence of redox processes is shown by a linear response, and charge storage is defined as the charge's adsorption at the electrode inference. When GCD is present, there is a significant IR decrease and a nonlinear curve. When discussing pseudocapacitors, the term "nonlinearity" refers to the charge-storage mechanism that results from oxidation and reduction reactions.

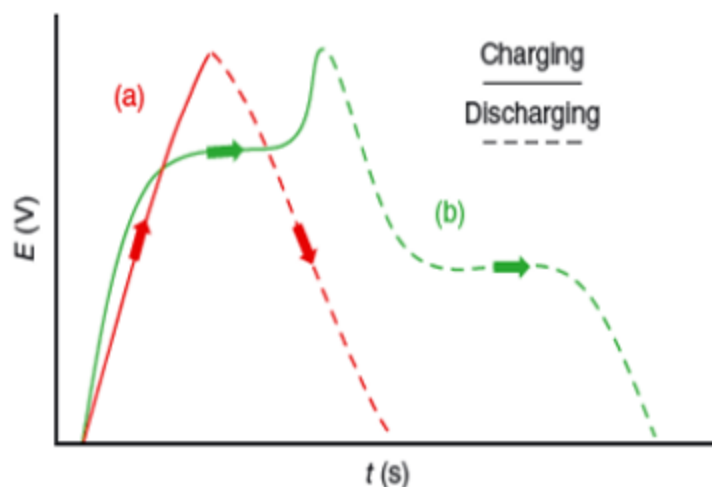


Figure 22: GCD curves of (a) EDLC (b) Pseudo capacitor [105].

#### 4.5.3 Cyclic Stability

A crucial component of energy storage devices is cyclic stability. Supercapacitors are subjected to several charge and discharge cycles to assess their cyclic performance. On a lab scale, 100–10,000 cycles of charge and discharge are often carried out to assess the material's capacity retention.

#### 4.5.4 Electrochemical Impedance Spectroscopy

An EIS determines the impedance of a material. As a function of frequency, it calculates the dielectric properties. There are two components to the EIS curve: a real axis and a semicircle. In an ideal scenario for a capacitive material, the semicircle should be smaller, and the real axis should be vertical. The curvature's shape in EIS is determined by the material's composition. The system's equivalent circuit response determines the Nyquist plot. Where  $R_{ct}$  is the polarization resistance or charge transfer resistance,  $R_e$  is the series resistance at the interface of working electrode and the electrolyte, Warburg impedance is dependent on reactant diffusion, and  $C_d$  is the double layer capacitance present at the interface of electrolyte and electrode.

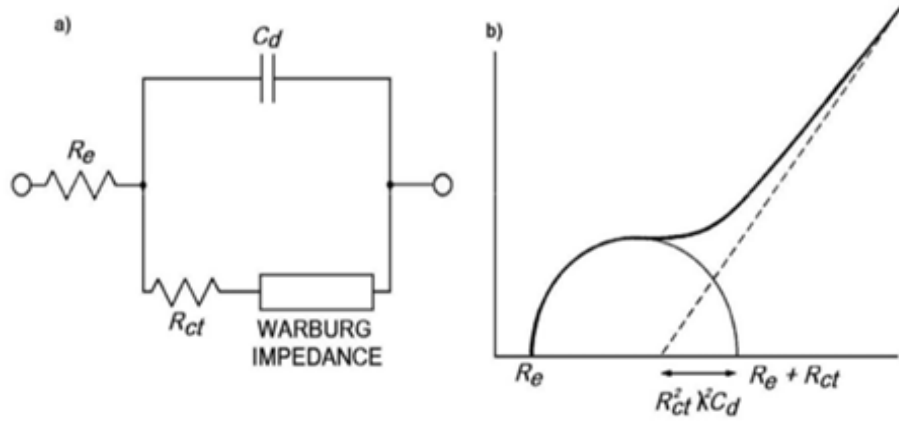


Figure 23: EIS (a) Equivalent circuit diagram (b) Nyquist plot [106].

## CHAPTER 5: RESULTS AND DISCUSSION

Literature review about energy storage devices show that compared to supercapacitors, the capacitance typically attained for batteries and fuel cells is higher. Supercapacitors, on the other hand, have a larger capacity than normal capacitors. Researchers have been studying new materials that can be utilized as electrodes to help supercapacitors overcome the issue of low capacitance.

In the current study, MXene, activated carbon and their composites were synthesized for supercapacitor applications to cope with the issue of low capacitance. MXene was synthesized using selective etching method, activated carbon was synthesized by KOH activation and their composites were made using physical mixing. This chapter provides a detailed introduction to electrochemical testing and characterization techniques used to evaluate the electrochemical performance of supercapacitor electrode materials.

### 5.1 XRD analysis

The XRD spectrum of MXene, AC, MAC1, MAC2 and MAC3 is shown in figure 24. The XRD spectra of MXene shows that after HF etching, the diffraction peak at  $38.6^\circ$  vanishes and the characteristic peak  $2\theta = 9.5^\circ$  corresponding to (002) plane is broadened and inclined to shift towards a lower angle of  $8.9^\circ$ . This shows that the lattice constant has changed and interplanar spacing has increased indicating that the MAX phase was successfully transformed to MXene. The XRD pattern of MXene shows peak at  $2\theta$  values of  $8.9^\circ$ ,  $18.3^\circ$ ,  $27.7^\circ$ ,  $34.4^\circ$ ,  $37.0^\circ$ ,  $41.5^\circ$ , and  $60.5^\circ$  which corresponds to (002), (004), (006), (008), (103), (105), and (110) planes respectively. The diffraction peaks of MXene are low in intensity and broader as compared to peaks in MAX phase, which indicates the successful etching of Al and an increased disorder in the crystal structure, these results are consistent with previously reported literature [94] [107]. The XRD spectrum of AC shows two broad non-crystalline peaks centered approximately at  $25^\circ$  and  $43.8^\circ$  which corresponds to (002) and (100) planes respectively, which is consistent with previous studies [108]. The less intense and broad humps confirm the amorphous structure of activated carbon and shows low degree of graphitization with a disordered carbon structure. The XRD spectra of all the composites MAC1, MAC2 and MAC3 shows that they possess all the

characteristic peaks of MXene and AC, except for the peak at 37.0° which is covered by a broad hump of AC ranging from 36-47, confirming the formation of MXene/AC composite. It is evident that all the peaks get less intense and broader as the amount of AC increases in the composite. This less intensity shows reduced crystallinity, and slight broadening of the peaks indicates further increase in the interlayer spacing as compared to MXene. Furthermore, this increase in disorder and peak broadening could also be attributed to the amorphous AC and high power ultrasonication used during composite preparation, which assisted the breaking of AC structure and Intercalation of AC between the MXene sheets. Overall, the composites have a graphitic microcrystalline amorphous carbon structure, which is consistent with the Raman results.

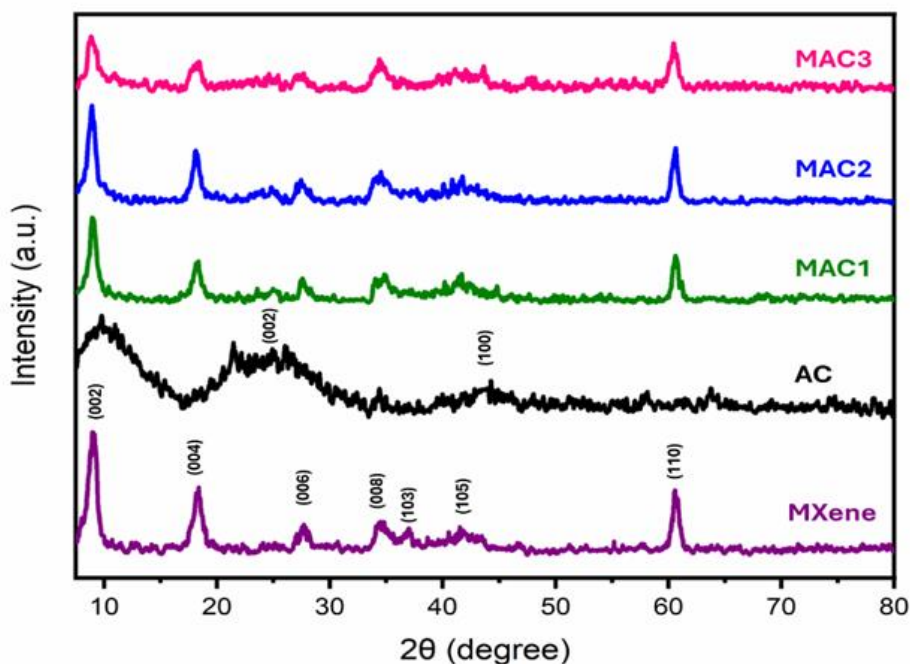


Figure 24: XRD pattern of MXene, AC, MAC1, MAC2 and MAC3.

## 5.2 Raman analysis

Figure 25 shows the Raman spectra of MXene, AC, MAC1, MAC2 and MAC3. The Raman spectrum of MXene shows a sharp peak at 157.8  $\text{cm}^{-1}$  and some low intensity peaks at 408.9  $\text{cm}^{-1}$  and 626.6  $\text{cm}^{-1}$  in the lower Raman shift range ( $<1000 \text{ cm}^{-1}$ ), which is because of the C-Ti



vibration, all of these peaks are significant features of MXene, similar to previously reported results [109]. On the other hand, AC shows two peaks at  $1364\text{ cm}^{-1}$  and  $1587\text{ cm}^{-1}$  which represents the D and G bands respectively. The D band shows the presence of defects and disorder, and the G band corresponds to the in-plane vibration, graphitization degree and symmetry of  $\text{sp}^2$  hybridization of carbon atoms, which is consistent with previous literature studies [110]. It can be seen from the spectra of AC that both peaks are sharp, showing defects and amorphous carbon ( $\text{sp}^3$  hybridization). The ratio of the D-band and G-band intensities, also called the  $I_D/I_G$  ratio, shows the degree of amorphization of the material. The larger the ratio, the higher the degree of disorder and amorphism and the lower the degree of graphitization. The  $I_D/I_G$  value of AC is 0.98 showing that it has a disordered structure with high density of defects and absence of a graphitic structure. The higher density of defects is key for enhancing capacitance. The Raman spectra of all the composites MAC1, MAC2 and MAC3 shows two characteristic peaks at  $1332\text{ cm}^{-1}$  and  $1575\text{ cm}^{-1}$  for MAC1,  $1352\text{ cm}^{-1}$  and  $1582\text{ cm}^{-1}$  for MAC2, and  $1364\text{ cm}^{-1}$  and  $1577\text{ cm}^{-1}$  for MAC3. It can be seen from the spectra that all the composites exhibit a sharp peak around  $151.9\text{ cm}^{-1}$  and a few peaks in the lower Raman shift region of low intensity, which belong to TiC vibrations from MXene. The  $I_D/I_G$  value of the composites are 0.84, 0.85 and 0.86 for MAC1, MAC2 and MAC3 respectively. These results imply that as the amount of AC increases in the composite, more defect sites are introduced, and the degree graphitization gets lowered as compared to MXene. This high degree of disorder and defects can provide more adsorption and active sites for better ion diffusion and charge transport, and provide lower resistance for electrochemical reactions to occur, thereby improving the capacitance of the material, which is consistent with the XRD results.

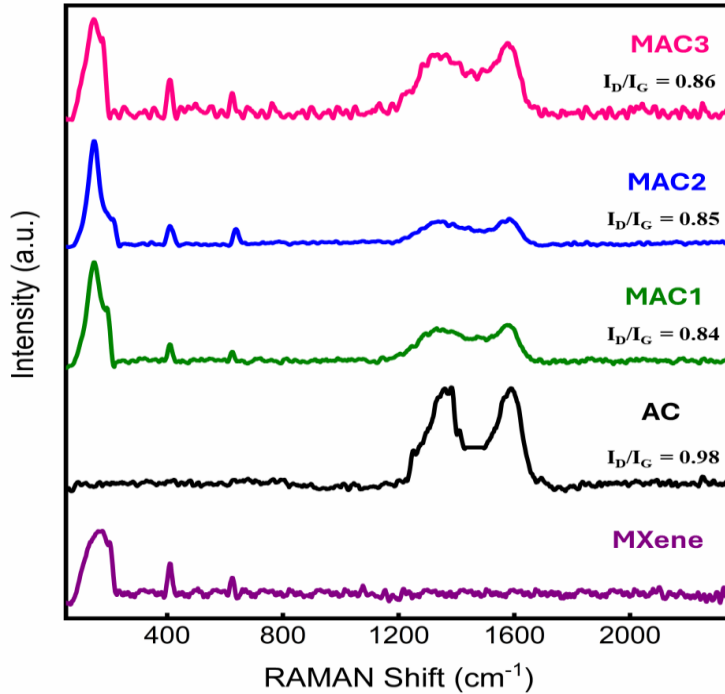


Figure 25: Raman plots of MXene, AC, MAC1, MAC2 and MAC3.

### 5.3 Brunauer Emmett Teller analysis

The specific surface and pore structure properties of the samples were investigated using N<sub>2</sub> adsorption analysis at 77 K, and the pore volume of the sample was calculated using the BJH model. Figure 26 shows the N<sub>2</sub> isotherms of MXene, AC and MAC1, MAC2 and MAC3. The isotherms of the samples revealed that AC had the highest BET surface area of 526.2 m<sup>2</sup>/g followed by the composites MAC3 with 140.2 m<sup>2</sup>/g, MAC2 with 117.1 m<sup>2</sup>/g and MAC1 with 82.4 m<sup>2</sup>/g. All these samples show values much higher than MXene which shows a BET surface area of 3.7 m<sup>2</sup>/g, similar to results reported in literature [111] [112]. From these results, it is evident that with addition of AC the surface area increases. As MAC3 has the most amount of AC, it exhibits a larger surface area than the other two composites. MAC1 has the smallest surface as it has the least amount of AC among the three composites. Pore volume of the samples was 0.2 cm<sup>3</sup>/g, 0.03 cm<sup>3</sup>/g, 0.05 cm<sup>3</sup>/g, 0.02 cm<sup>3</sup>/g and 0.007cm<sup>3</sup>/g for AC, MAC3, MAC2, MAC1 and MXene respectively. Pore volume or pore size distribution indicates that AC has a macroporous structure. The BET results for the specific surface area and pore volume of all

composites were between AC and MXene, which is because MXene is very small and can cover or block some pores and large AC particles. On the one hand, the addition of AC between MXene sheets increases the surface area of the material compared to pure MXene, which is due to the porous nature of AC. The results show that the composite has a 3D macroporous structure, which is consistent with the SEM analysis. The presence of this high surface area porous structure not only ensures numerous active sites on the MXene layers but also facilitates smooth and rapid ion transport. This property is of great importance for improving electrochemical performance and suppressing interfacial reactions that occur between electrolytes and electrode materials.

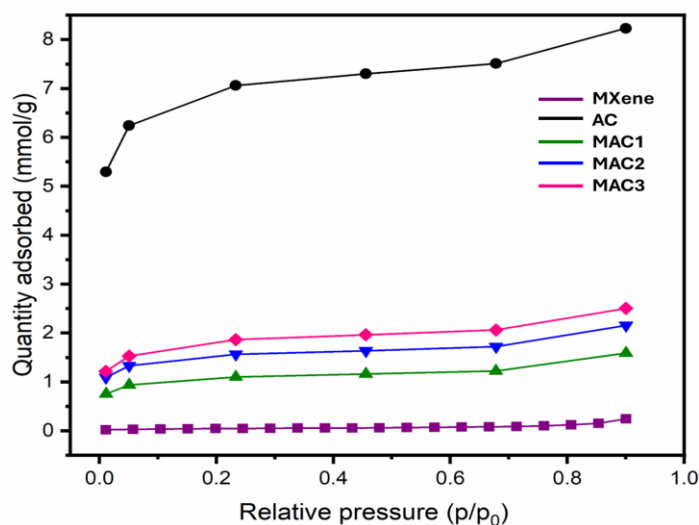
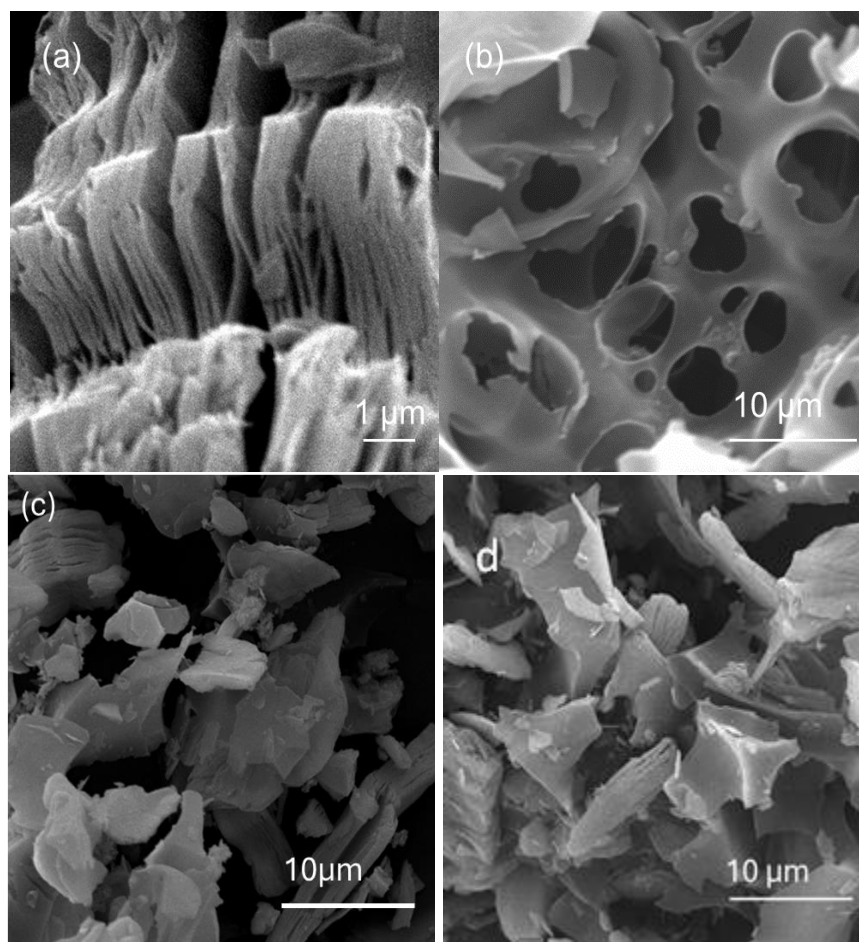


Figure 26: BET plot of MXene, AC, MAC1, MAC2 and MAC3.

#### 5.4 SEM analysis

The microstructure and morphology of MXene, AC, MAC1, MAC2 and MAC3 were characterized using SEM. As shown in image in figure 27(a), the dense close packed structure of MAX phase has transformed into an accordion-like structure of open stacked thin sheets, similar to results reported in previous studies [113]. This two-dimensional structure of MXene depicts successful exfoliation of Al after HF etching. The multilayered structure of MXene provides good conductivity and high surface area. On the other hand, AC has a porous structure with a

rough surface and numerous holes, which is consistent with the results in the literature [114]. The macropores in AC can facilitate rapid ion diffusion, electron transfer and charge storage. Figure 27(c-e) shows that the composites combine these features and displays a three-dimensional conductive network, where MXene sheets are uniformly dispersed within the AC macroporous structure. Additionally, the embedding of some tiny particles of AC hindered the restacking of MXene layers, which in turns increases the active sites available for electrolyte ion transport. A variation in the amount of AC can also be observed from the images as we go from MAC1 to MAC3. This three-dimensional conductive network is a well-integrated structure in which the two-dimensional nanosheets provide better conductivity due to high surface area between the sheets and the macropores provide abundant channels for the adsorption of electrolyte ions. This composite structure suggests an enhanced electrochemical performance, which makes it a suitable electrode material.



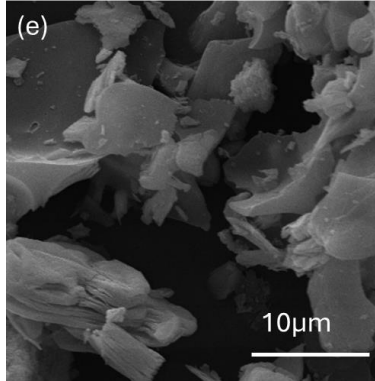


Figure 27: SEM images of (a) MXene, (b) AC, (c) MAC1, (d) MAC2 and (e) MAC3.

## 5.5 Electrochemical Characterization

All electrochemical tests, including cyclic voltammetry (CV), electrochemical impedance spectroscopy (EIS), and galvanostatic charge and discharge (GCD), were performed on a Gamry 1010E electrochemical workstation. Electrochemical measurements were performed in a three-electrode system in 3M KOH electrolyte. The prepared electrode was used as the working electrode, the platinum wire as the counter electrode, and the Ag/AgCl electrode as the reference electrode. Cyclic voltammetric analysis was performed in a potential window range of 0V – 0.6 V at a sampling rate of 5 to 100 mV/s. EIS analysis was carried out in the frequency range 0.1 – 100 kHz. Galvanostatic charging and discharging occurs at a current density of 0.5 to 10 A/g in the potential range of 0-0.45 V. The specific capacitance of the electrode was calculated using the following equation [115]:

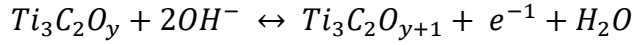
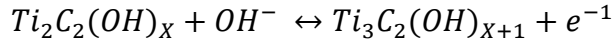
$$C_s = \frac{I \times \Delta t}{m \times \Delta V}$$

Where, I is the test current (A),  $\Delta t$  is the discharge time (s), m is the mass of the active material (g), and  $\Delta V$  is the voltage window (V).

## 5.6 Cyclic Voltammetry (CV)

Figure 28(a) shows the CV curves of MXene, AC and composites materials at 5 mV/s. All samples exhibit a pair of obvious redox peaks, illustrating the pseudocapacitive behavior. These

redox peaks in MXene can be attributed to the adsorption and desorption of -OH on the MXene surface from the KOH electrolyte. Redox reaction takes place due to the following reaction [81]:



In AC, in addition to the adsorption and desorption of electrolyte ions, the appearance of the hump is due to the redox reaction which is caused by present functional groups on AC's surface such as hydroxyl, carbonyl and carboxyl groups, which are introduced during the KOH activation process. Since the composite material combines these properties of MXene and AC, redox peaks occur in both of the above-mentioned processes. The specific capacitance of the samples at 5 mV/s was 588.35 F/g, 939 F/g, 645.05 F/g, 738.95 F/g and 1080 F/g for MXene, AC, MAC1, MAC2 and MAC3 respectively. It is also apparent from the CV curves that MAC3 has the largest area compared to all the samples, indicating the highest capacitance value. This can be accredited to high amount of AC present as compared to MAC1 and MAC2. This is due to the synergistic effect of the MXene/AC conductive network, which combines the large surface area of thin nanosheets that facilitate surface adsorption/desorption with the porous structure that provides channels for fast ion transport. MAC1 and MAC2 show lower capacitance than MAC3 and AC, this may be due to presence of less amount of AC and, due to small size of MXene that may have blocked some of the pores of AC, thereby reducing the available active sites in the material. Table 2 shows the specific capacitance values of MXene, AC, MAC1, MAC2 and MAC3 at different scan rates. Figure 28(b-f) shows the CV curves for all samples in the range 5-100 mV/s. From the CV curves of all samples, it can be seen that the redox peaks move to higher potential values and lower potential values with increasing scan rate, respectively, and the shape of the CV curves does not change significantly, indicating that the redox reaction has good reversibility on.

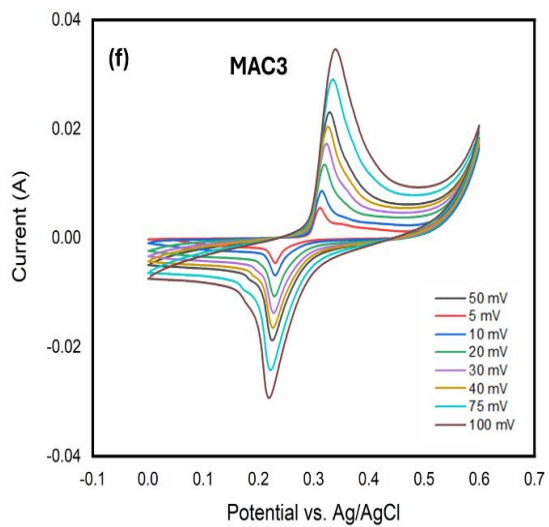
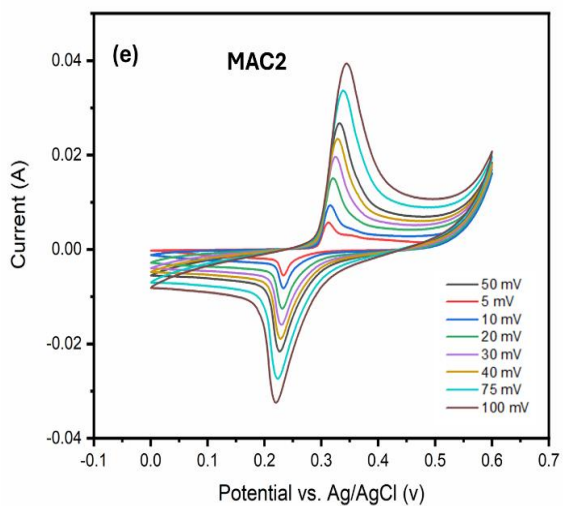
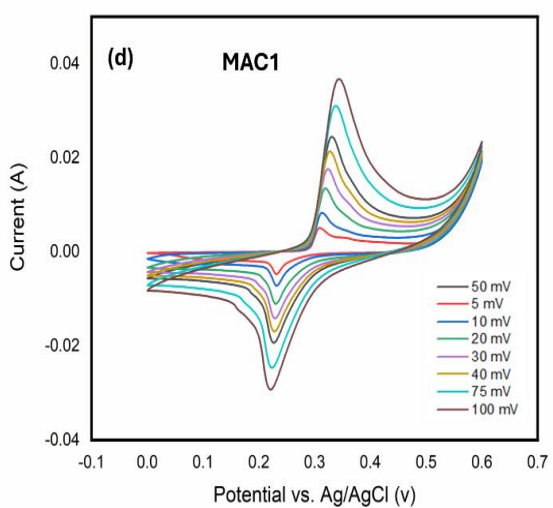
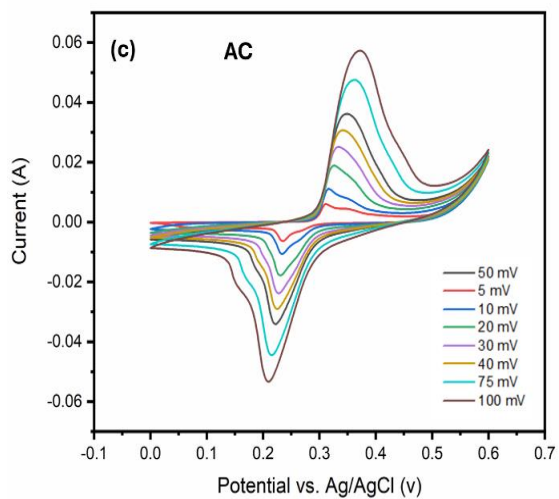
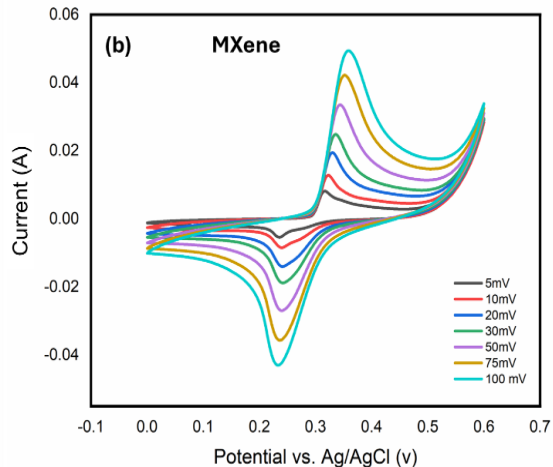
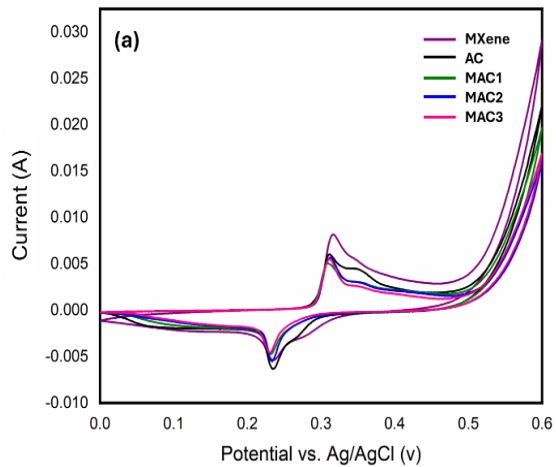


Figure 28: Cyclic voltammograms of (a) all samples at 5mV/s, (b) MXene at various scan rates, (c) AC at various scan rates, (d) MAC1 at various scan rates, (e) MAC2 at various scan rates and (f) MAC3 at various scan rates.

Table 2: Specific capacitance of all samples calculated from CV data.

Scan rate	Specific Capacitance (F/g)				
	MXene	AC	MAC1	MAC2	MAC3
5 mV/s	588.358	9.39E+02	645.0526	738.9525	1.08E+03
10 mV/s	448.1462	7.94E+02	525.1416	598.8529	8.96E+02
20 mV/s	337.6301	6.37E+02	396.5599	469.167	7.11E+02
30 mV/s	290.4175	5.70E+02	333.5044	396.1514	6.02E+02
40 mV/s	-	5.28E+02	297.1818	352.6637	5.42E+02
50 mV/s	245.1091	5.03E+02	275.0058	328.5808	4.96E+02
75 mV/s	218.9546	4.68E+02	244.5244	288.8234	4.33E+02
100 mV/s	201.7035	4.46E+02	227.1043	267.3622	3.99E+02



To study the charge storage mechanisms and dynamics of active materials, the following relationship, called the power law, is used:

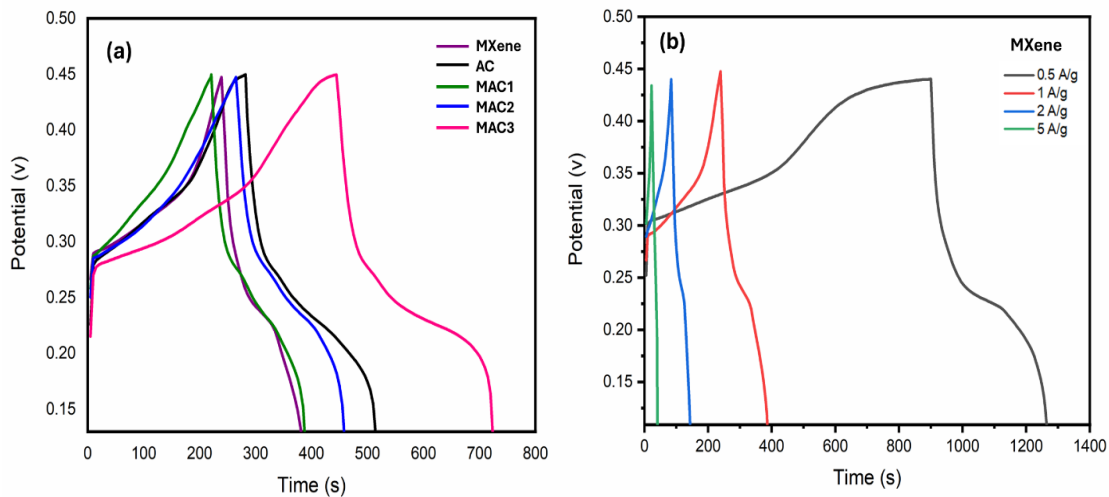
$$I(V) = av^b$$

Where  $I(V)$  is the peak current,  $v$  is the sampling rate and  $a$  and  $b$  are constants. The  $b$  value is determined by plotting  $\log(I(V))$  against  $\log(v)$ . In general, for  $b$ -value fitting calculations,  $b = 0.5$  means that the electrochemical process is a diffusion-controlled process, while  $b = 1$  indicates that the electrochemical process has capacitive behavior [116]. The charge storage mechanism in electrodes consists of two different components: diffusion-controlled and non-diffusion-controlled. Diffusion-limited processes occur when the transfer of ions of electrolyte across the surface of electrode becomes the limiting factor of the electrochemical reaction. The capacitive behavior is controlled during electrochemical processes by Faraday charge transfer and ion adsorption at the interface between electrode material and electrolyte. The  $b$ -value MXene, MAC1, MAC2, MAC3 and AC was 0.80, 0.84, 0.89, 0.89 and 0.98 respectively. The high  $b$ -value of AC as compared to MXene and MAC, indicates that it predominantly exhibits a capacitive behavior with negligible contribution of diffusion-controlled process, this can be attributed to the fact that AC has abundant macropores which provides plenty of channels for ion adsorption and desorption even at the interface of electrode and electrolyte. MXene and all the composites show both pseudocapacitive and battery-like behavior. All the composites, however, show a  $b$ -value between MXene and AC, this is due to the addition of AC in MXene, the pore size distribution increased, and the composite became conducive to large storage, rapid ion transfer on the surface as well as diffusion of ions inside the material. This synergistic effect increased the capacitive behavior of the electrode material with little contribution of diffusion-controlled process, this result is consistent with the BET results discussed earlier.

## 5.7 Galvanostatic Charge Discharge (GCD)

Figure 29(a) shows the GCD curves of MXene, AC, MAC1, MAC2 and MAC3 at 1 A/g. MAC3 showed longer charge/discharge times compared to all samples, indicating higher charge storage capability. The specific capacitance value of MXene, AC, MAC1, MAC2 and MAC3 determined

at 1 A/g is 280 F/g, 442 F/g, 318.4 F/g, 364.2 F/g and 540 F/g respectively. Compared with MXene and AC, the high specific capacity of MAC3 can be ascribed to a few reasons including: (i) The 2D/3D hierarchical structure provides abundant active sites, which facilitates rapid ion diffusion. (ii) There is an optimal amount of alternating current. (iii) The porous structure associated with thin nanosheets has a large surface area and large pore volume, which can improve the ion dynamics at the electrode-electrolyte interface. Figure 29 shows the GCD curves of all samples at different current densities. The potential plateau visible in the curves corresponds to the redox process, which means that the sample shows pseudocapacitive behavior, which is consistent with the CV results. As the current density increases, the charge-discharge cycle time shortens, which may be due to the lower utilization of active materials at high current densities [117]. Furthermore, the specific capacitance decreases with increasing current density, which is due to the slow diffusion of ions through the electrode at higher current densities. From Figure 29(b-f), it can be seen that the symmetry of the curve indicates high Coulomb efficiency. The reason for the improved electrochemical performance of the composites compared to MXene can be attributed to the three-dimensional network with interconnected two-dimensional nanostructures, which provides a large surface area and creates short paths for electrolyte ion transport. Furthermore, AC is the backbone for faster transport and optimal interactions between MXene and ions.



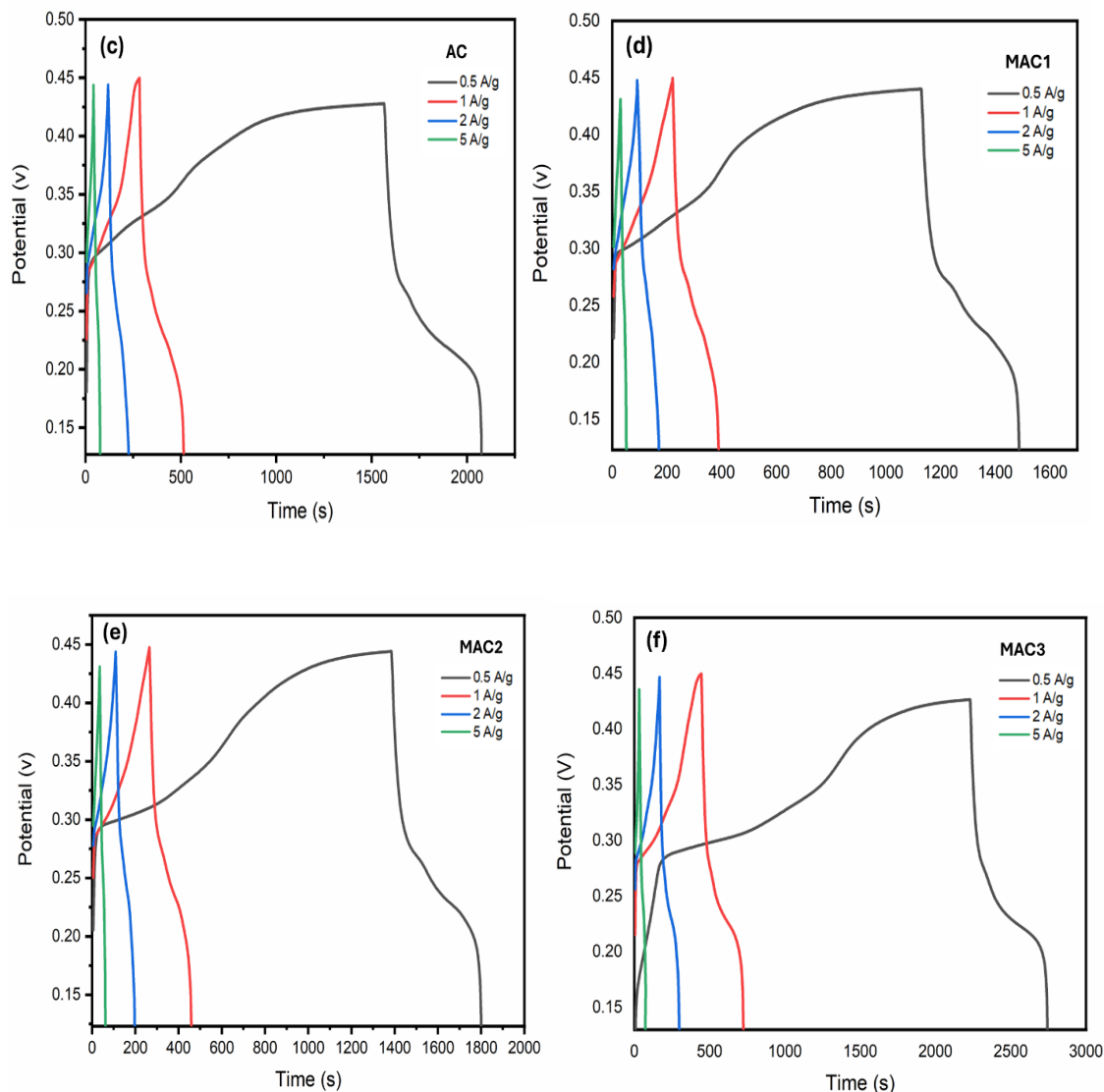


Figure 29: GCD curves of (a) All samples at 1 A/g, (b) MXene at different current densities, (c) AC at different current densities, (d) MAC1 at different current densities, (e) MAC2 at different current densities, (f) MAC3 at different current densities.

## 5.8 Electrochemical impedance Spectroscopy (EIS)

To further investigate the electrochemical properties of MXene, AC and composites, EIS measurements were carried out. Figure 30 shows the Nyquist diagrams of MXene, AC, MAC1, MAC2 and MAC3. Nyquist diagrams have low frequency regions and high frequency regions. The high frequency range consists of a semicircular arc that corresponds to the charge transfer resistance. The real axis's intersection point and the semicircular arc corresponds to the

equivalent series resistance [118]. The low frequency range represents the contribution of capacitive behavior. A typical slope close to 45 in the medium frequency range corresponds to the Warburg impedance and indicates the contribution of diffusion-related processes. From the high frequency region, the obtained  $R_s$  value of MXene, AC and MAC was 0.44  $\Omega$ , 0.46  $\Omega$ , 0.47  $\Omega$ , 0.46  $\Omega$  and 0.47  $\Omega$  respectively. These  $R_s$  values indicate very low ohmic resistance between the contactable area of electrode and electrolyte, enhanced charge-transfer kinetics and efficient ion diffusion tunnels. The slight increase in the resistance value of the composite may be due to the fact that some large AC pores may be covered or blocked by MXene sheets because the size of MXene is very small, which is consistent with the BET results. The low frequency range shows a very small Warburg impedance value of 0.03 for the composite, indicating efficient ion transport. This is due to the three-dimensional conductive structure with large surface area and high porosity, which provides an easy path for ion diffusion.

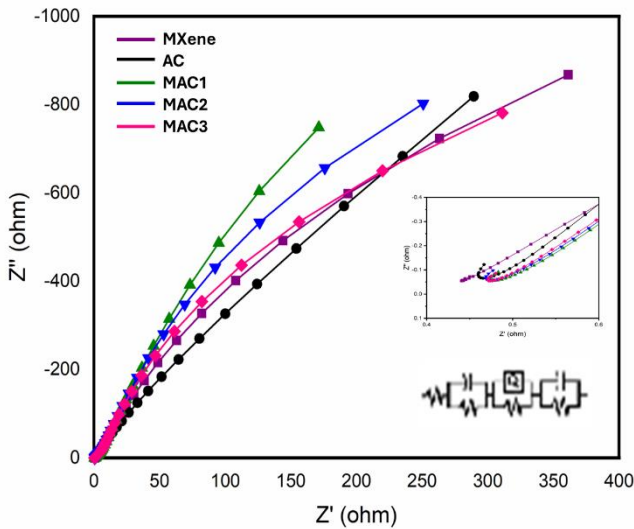


Figure 30: Nyquist plots of MXene, AC, MAC1, MAC2 and MAC3.

Figure 31 shows the Bode phase angle diagrams of MXene, AC and composites. The Bode phase angle provides information about the electrochemical behavior of electrode materials. A phase angle of  $-90^\circ$  near the low frequency region represents an ideal capacitor, a phase angle of  $0^\circ$  near the high frequency region represents resistance losses, and a phase angle between  $45^\circ$  and  $60^\circ$  in the transition region represents a mixed capacitor behavior of capacitance and resistance. The

phase angle of MXene, AC, MAC1, MAC2 and MAC3 found from the Bode phase angle plot was  $-67.3^\circ$ ,  $-70.5^\circ$ ,  $-77.1^\circ$ ,  $-72.6^\circ$  and  $-68.2^\circ$  respectively. All the samples show phase angles that represent a significant capacitive behavior. These values indicate the pseudocapacitive behavior of the samples. It is evident from the results that all the materials have excellent electrochemical performance, with minimal resistive losses and fast charging/discharging. This outstanding electrochemical performance is because of the introduction of alternating current, which acts as a porous conveyor belt and spacer between MXene plates, providing conductivity. Overall, this three-dimensional conductive network improves the mobility of electrolyte ions which makes it a suitable electrode material for efficient storage and delivery of energy.

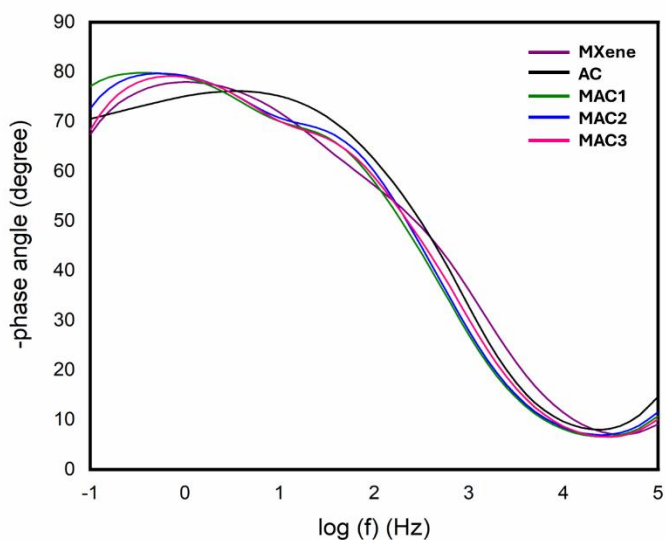


Figure 31: Bode phase angle plot of MXene, AC, MAC1, MAC2 and MAC3.

## 5.9 Cycle Stability

Cycling stability is a fundamental requirement for characterizing materials for practical supercapacitor applications. We performed a stability test on the best sample, MAC3. The stability test was carried out by repeating 300 GCD cycles at current density of 5 A/g. The specific capacity gradually decreased, and the capacity retention rate was still 81.1% after 300 cycles, showing good cycling stability. The decrease in specific capacity may be due to the clogging of some pores and available active sites after a few cycles [93]. After 300 cycles, the

Coulombic efficiency of MAC3 was 98.5%, indicating that the redox reaction has excellent rate and reversibility. The results show that MAC3 has excellent electrochemical properties and has potential as an electrode material for supercapacitor application.

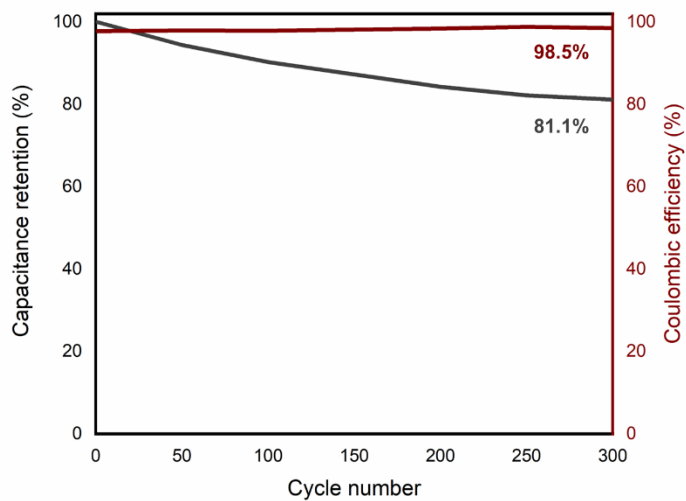


Figure 32: Cycle stability and Coulombic efficiency plot of MAC3.

## CHAPTER 6: CONCLUSION

In the present study, MXene was successfully synthesized through selective etching method, activated carbon was activated through KOH activation and their composites were prepared by physical mixing. Furthermore, compositional, microstructure, morphological, surface area and electrochemical properties were investigated. XRD analysis was carried out to examine the crystal structure of the samples. XRD results of MXene showed successful etching of Al, confirming its successful transformation from the MAX phase. XRD of AC showed an amorphous structure, which confirmed the formation of MXene/AC composite, as the structure of the composite had all the characteristic peaks of MXene and exhibited peak shifts due to amorphous AC. Raman analysis is performed to examine the level of disorder and graphitization in the sample. The results showed that AC has an  $I_D/I_G$  value of 0.98 which indicates the absence of graphitic structure and high degree of disorder. Further the composites showed an  $I_D/I_G$  value of 0.84, 0.85 and 0.86 for MAC1, MAC2 and MAC3 respectively, which shows the increase in disorder as AC content increases in the composites. The surface area and pore size were examined by BET analysis. The surface area of MXene was  $3.7 \text{ m}^2/\text{g}$ , AC had a specific surface area of  $526.2 \text{ m}^2/\text{g}$ , while the composites showed surface areas of  $82.4 \text{ m}^2/\text{g}$ ,  $117.1 \text{ m}^2/\text{g}$  and  $140.2 \text{ m}^2/\text{g}$  by MAC1, MAC2 and MAC3, respectively. These results suggest that the surface area increases when AC is introduced into MXene. The microstructure and morphology of the samples were analyzed using scanning electron microscopy (SEM). SEM results of MXene showed an accordion like structure which confirmed its synthesis, results of AC showed a highly porous structure, and the composites showed a three-dimensional network, where MXene sheets are uniformly dispersed within the AC macroporous structure. Electrochemical characterization was performed to investigate the electrochemical performance of the samples as supercapacitor electrode materials. Electrochemical results show that the synthesized material has good supercapacitive behavior, which is attributed to the synergistic performance of MXene and activated carbon. MAC3 has a high specific capacitance of  $1080 \text{ F/g}$  at a scan rate of  $5 \text{ mV/s}$ , which is higher than both the parent materials MXene and AC. Furthermore, MAC3 showed good cycling stability of  $81.1\%$  and Coulombic efficiency of  $98.5\%$  after 300 cycles. These

results suggest that MAC3 has excellent electrochemical properties as a promising electrode material for supercapacitors.



## REFERENCES

- [1] K. K. Upadhyay *et al.*, “Capacitance response in an aqueous electrolyte of Nb<sub>2</sub>O<sub>5</sub> nanochannel layers anodically grown in pure molten o-H<sub>3</sub>PO<sub>4</sub>,” *Electrochimica Acta*, vol. 281, pp. 725–737, Aug. 2018, doi: 10.1016/j.electacta.2018.06.014.
- [2] A. González, E. Goikolea, J. A. Barrena, and R. Mysyk, “Review on supercapacitors: Technologies and materials,” *Renew. Sustain. Energy Rev.*, vol. 58, pp. 1189–1206, May 2016, doi: 10.1016/j.rser.2015.12.249.
- [3] A. Dutta, S. Mitra, M. Basak, and T. Banerjee, “A comprehensive review on batteries and supercapacitors: Development and challenges since their inception,” *Energy Storage*, vol. 5, no. 1, p. e339, Feb. 2023, doi: 10.1002/est2.339.
- [4] M. Winter and R. J. Brodd, “What Are Batteries, Fuel Cells, and Supercapacitors?,” *Chem. Rev.*, vol. 104, no. 10, pp. 4245–4270, Oct. 2004, doi: 10.1021/cr020730k.
- [5] K. Gunawardane, N. Bandara, K. Subasinghage, and N. Kularatna, “Extending the Input Voltage Range of Solar PV Inverters with Supercapacitor Energy Circulation,” *Electronics*, vol. 10, no. 1, p. 88, Jan. 2021, doi: 10.3390/electronics10010088.
- [6] Z. S. Iro, C. Subramani, and S. S. Dash, “A Brief Review on Electrode Materials for Supercapacitor,” *Int. J. Electrochem. Sci.*, vol. 11, no. 12, pp. 10628–10643, Dec. 2016, doi: 10.20964/2016.12.50.
- [7] A. Achour *et al.*, “Titanium vanadium nitride electrode for micro-supercapacitors,” *Electrochem. Commun.*, vol. 77, pp. 40–43, Apr. 2017, doi: 10.1016/j.elecom.2017.02.011.
- [8] R. Kötz and M. Carlen, “Principles and applications of electrochemical capacitors,” *Electrochimica Acta*, vol. 45, no. 15–16, pp. 2483–2498, May 2000, doi: 10.1016/S0013-4686(00)00354-6.
- [9] “XL60 Supercapacitors.” Accessed: Oct. 09, 2024. [Online]. Available: <https://www.mouser.ee/eaton-xl60-supercapacitors>
- [10] Oyedotun Kabir Oyeniran, “Synthesis and characterization of carbon-based nanostructured material electrodes for designing novel hybrid supercapacitors,” 2018, doi: 10.13140/RG.2.2.20007.50084.
- [11] A. Joseph and T. Thomas, “Pseudocapacitance: An Introduction,” in *Pseudocapacitors*, R. K. Gupta, Ed., in Engineering Materials. , Cham: Springer Nature Switzerland, 2024, pp. 1–17. doi: 10.1007/978-3-031-45430-1\_1.

- [12] R. Reece, C. Lekakou, and P. A. Smith, “A High-Performance Structural Supercapacitor,” *ACS Appl. Mater. Interfaces*, vol. 12, no. 23, pp. 25683–25692, Jun. 2020, doi: 10.1021/acsami.9b23427.
- [13] M. Jasna, M. P. Manoj, and M. K. E. Jayaraj, “Carbon Based Composites for Supercapacitor Applications,” in *Energy Harvesting and Storage*, M. K. Jayaraj, A. Antony, and P. P. Subha, Eds., in Energy Systems in Electrical Engineering. , Singapore: Springer Nature Singapore, 2022, pp. 259–284. doi: 10.1007/978-981-19-4526-7\_9.
- [14] A. Chandra, “Supercapacitors: An Alternate Technology for Energy Storage,” *Proc. Natl. Acad. Sci. India Sect. Phys. Sci.*, vol. 82, no. 1, pp. 79–90, Mar. 2012, doi: 10.1007/s40010-012-0009-9.
- [15] M. Sarno, “Nanotechnology in energy storage: the supercapacitors,” in *Studies in Surface Science and Catalysis*, vol. 179, Elsevier, 2020, pp. 431–458. doi: 10.1016/B978-0-444-64337-7.00022-7.
- [16] D. P. Chatterjee and A. K. Nandi, “A review on the recent advances in hybrid supercapacitors,” *J. Mater. Chem. A*, vol. 9, no. 29, pp. 15880–15918, 2021, doi: 10.1039/D1TA02505H.
- [17] A. Muzaffar, M. B. Ahamed, K. Deshmukh, and J. Thirumalai, “A review on recent advances in hybrid supercapacitors: Design, fabrication and applications,” *Renew. Sustain. Energy Rev.*, vol. 101, pp. 123–145, Mar. 2019, doi: 10.1016/j.rser.2018.10.026.
- [18] A. Burke, Z. Liu, and H. Zhao, “Present and future applications of supercapacitors in electric and hybrid vehicles,” in *2014 IEEE International Electric Vehicle Conference (IEVC)*, Florence: IEEE, Dec. 2014, pp. 1–8. doi: 10.1109/IEVC.2014.7056094.
- [19] I. Shown, A. Ganguly, L. Chen, and K. Chen, “Conducting polymer-based flexible supercapacitor,” *Energy Sci. Eng.*, vol. 3, no. 1, pp. 2–26, Jan. 2015, doi: 10.1002/ese3.50.
- [20] Reenu, Sonia, L. Phor, A. Kumar, and S. Chahal, “Electrode materials for supercapacitors: A comprehensive review of advancements and performance,” *J. Energy Storage*, vol. 84, p. 110698, Apr. 2024, doi: 10.1016/j.est.2024.110698.
- [21] R. Dubey and V. Guruviah, “Review of carbon-based electrode materials for supercapacitor energy storage,” *Ionics*, vol. 25, no. 4, pp. 1419–1445, Apr. 2019, doi: 10.1007/s11581-019-02874-0.
- [22] T. Zhao *et al.*, “In situ synthesis of interlinked three-dimensional graphene foam/polyaniline nanorod supercapacitor,” *Electrochimica Acta*, vol. 230, pp. 342–349, Mar. 2017, doi: 10.1016/j.electacta.2017.02.021.
- [23] A. Asghar *et al.*, “Recent progress in metal oxide-based electrode materials for safe and sustainable variants of supercapacitors,” *Front. Chem.*, vol. 12, p. 1402563, May 2024, doi: 10.3389/fchem.2024.1402563.

- [24] Z. Roohi, F. Mighri, and Z. Zhang, “Conductive Polymer-Based Electrodes and Supercapacitors: Materials, Electrolytes, and Characterizations,” *Materials*, vol. 17, no. 16, p. 4126, Aug. 2024, doi: 10.3390/ma17164126.
- [25] R. Yang *et al.*, “Development and challenges of electrode materials for rechargeable Mg batteries,” *Energy Storage Mater.*, vol. 42, pp. 687–704, Nov. 2021, doi: 10.1016/j.ensm.2021.08.019.
- [26] M. K. Muhamad Azim, A. Arifuzzaman, R. Saidur, M. U. Khandaker, and D. A. Bradley, “Recent progress in emerging hybrid nanomaterials towards the energy storage and heat transfer applications: A review,” *J. Mol. Liq.*, vol. 360, p. 119443, Aug. 2022, doi: 10.1016/j.molliq.2022.119443.
- [27] C. Lamiel, I. Hussain, J. H. Warner, and K. Zhang, “Beyond Ti-based MXenes: A review of emerging non-Ti based metal-MXene structure, properties, and applications,” *Mater. Today*, vol. 63, pp. 313–338, Mar. 2023, doi: 10.1016/j.mattod.2023.01.020.
- [28] M. Pogorielov, K. Smyrnova, S. Kyrylenko, O. Gogotsi, V. Zahorodna, and A. Pogrebnjak, “MXenes—A New Class of Two-Dimensional Materials: Structure, Properties and Potential Applications,” *Nanomaterials*, vol. 11, no. 12, p. 3412, Dec. 2021, doi: 10.3390/nano11123412.
- [29] S. Asad *et al.*, “Recent Advances in Titanium Carbide MXene ( $\text{Ti}_3\text{C}_2\text{T}_x$ ) Cathode Material for Lithium–Air Battery,” *ACS Appl. Energy Mater.*, vol. 5, no. 10, pp. 11933–11946, Oct. 2022, doi: 10.1021/acsaem.2c01845.
- [30] W. Hong, B. C. Wyatt, S. K. Nemani, and B. Anasori, “Double transition-metal MXenes: Atomistic design of two-dimensional carbides and nitrides,” *MRS Bull.*, vol. 45, no. 10, pp. 850–861, Oct. 2020, doi: 10.1557/mrs.2020.251.
- [31] Y. Yu, Q. Fan, Z. Li, and P. Fu, “MXene-based electrode materials for supercapacitors: Synthesis, properties, and optimization strategies,” *Mater. Today Sustain.*, vol. 24, p. 100551, Dec. 2023, doi: 10.1016/j.mtsust.2023.100551.
- [32] M. R. Lukatskaya *et al.*, “Cation Intercalation and High Volumetric Capacitance of Two-Dimensional Titanium Carbide,” *Science*, vol. 341, no. 6153, pp. 1502–1505, Sep. 2013, doi: 10.1126/science.1241488.
- [33] S. Nahirniak, A. Ray, and B. Saruhan, “Challenges and Future Prospects of the MXene-Based Materials for Energy Storage Applications,” *Batteries*, vol. 9, no. 2, p. 126, Feb. 2023, doi: 10.3390/batteries9020126.
- [34] J. L. Ramos, B. Pakuts, P. Godoy, A. García-Franco, and E. Duque, “Addressing the energy crisis: using microbes to make biofuels,” *Microb. Biotechnol.*, vol. 15, no. 4, pp. 1026–1030, Apr. 2022, doi: 10.1111/1751-7915.14050.

- [35] N. Dahmen, I. Lewandowski, S. Zibek, and A. Weidtmann, “Integrated lignocellulosic value chains in a growing bioeconomy: Status quo and perspectives,” *GCB Bioenergy*, vol. 11, no. 1, pp. 107–117, Jan. 2019, doi: 10.1111/gcbb.12586.
- [36] R. Kumar *et al.*, “Lignocellulose biomass pyrolysis for bio-oil production: A review of biomass pre-treatment methods for production of drop-in fuels,” *Renew. Sustain. Energy Rev.*, vol. 123, p. 109763, May 2020, doi: 10.1016/j.rser.2020.109763.
- [37] Y. Zhang, H. Pan, Q. Zhou, K. Liu, W. Ma, and S. Fan, “Biomass-derived carbon for supercapacitors electrodes – A review of recent advances,” *Inorg. Chem. Commun.*, vol. 153, p. 110768, Jul. 2023, doi: 10.1016/j.inoche.2023.110768.
- [38] M. Gayathiri, T. Pulingam, K. T. Lee, and K. Sudesh, “Activated carbon from biomass waste precursors: Factors affecting production and adsorption mechanism,” *Chemosphere*, vol. 294, p. 133764, May 2022, doi: 10.1016/j.chemosphere.2022.133764.
- [39] Z. Gao, Y. Zhang, N. Song, and X. Li, “Biomass-derived renewable carbon materials for electrochemical energy storage,” *Mater. Res. Lett.*, vol. 5, no. 2, pp. 69–88, Mar. 2017, doi: 10.1080/21663831.2016.1250834.
- [40] E. Huarote-Garcia *et al.*, “Activated Carbon Electrodes for Supercapacitors from Purple Corn cob ( *Zea mays L.* ),” *ACS Environ. Au*, vol. 4, no. 2, pp. 80–88, Mar. 2024, doi: 10.1021/acsenvironau.3c00048.
- [41] A. Ahmad *et al.*, “Preparation and Characterization of Physically Activated Carbon and Its Energetic Application for All-Solid-State Supercapacitors: A Case Study,” *ACS Omega*, vol. 8, no. 24, pp. 21653–21663, Jun. 2023, doi: 10.1021/acsomega.3c01065.
- [42] P. Manasa, S. Sambasivam, and F. Ran, “Recent progress on biomass waste derived activated carbon electrode materials for supercapacitors applications—A review,” *J. Energy Storage*, vol. 54, p. 105290, Oct. 2022, doi: 10.1016/j.est.2022.105290.
- [43] S. Saini, P. Chand, and A. Joshi, “Biomass derived carbon for supercapacitor applications: Review,” *J. Energy Storage*, vol. 39, p. 102646, Jul. 2021, doi: 10.1016/j.est.2021.102646.
- [44] A. Afif, S. M. Rahman, A. Tasfiah Azad, J. Zaini, M. A. Islan, and A. K. Azad, “Advanced materials and technologies for hybrid supercapacitors for energy storage – A review,” *J. Energy Storage*, vol. 25, p. 100852, Oct. 2019, doi: 10.1016/j.est.2019.100852.
- [45] C.-C. Hu, J.-C. Chen, and K.-H. Chang, “Cathodic deposition of Ni(OH)<sub>2</sub> and Co(OH)<sub>2</sub> for asymmetric supercapacitors: Importance of the electrochemical reversibility of redox couples,” *J. Power Sources*, vol. 221, pp. 128–133, Jan. 2013, doi: 10.1016/j.jpowsour.2012.07.111.
- [46] X. Chen, R. Paul, and L. Dai, “Carbon-based supercapacitors for efficient energy storage,” *Natl. Sci. Rev.*, vol. 4, no. 3, pp. 453–489, May 2017, doi: 10.1093/nsr/nwx009.

- [47] H.-L. Girard, H. Wang, A. d'Entremont, and L. Pilon, "Physical Interpretation of Cyclic Voltammetry for Hybrid Pseudocapacitors," *J. Phys. Chem. C*, vol. 119, no. 21, pp. 11349–11361, May 2015, doi: 10.1021/acs.jpcc.5b00641.
- [48] S. Gupta and C. Price, "Investigating graphene/conducting polymer hybrid layered composites as pseudocapacitors: Interplay of heterogeneous electron transfer, electric double layers and mechanical stability," *Compos. Part B Eng.*, vol. 105, pp. 46–59, Nov. 2016, doi: 10.1016/j.compositesb.2016.08.035.
- [49] Y. Ma, H. Chang, M. Zhang, and Y. Chen, "Graphene-Based Materials for Lithium-Ion Hybrid Supercapacitors," *Adv. Mater.*, vol. 27, no. 36, pp. 5296–5308, Sep. 2015, doi: 10.1002/adma.201501622.
- [50] H. Zhou and J. He, "Synthesis of the New High Entropy Alloy and Its Application in Energy Conversion and Storage," *Front. Energy Res.*, vol. 8, p. 73, Jun. 2020, doi: 10.3389/fenrg.2020.00073.
- [51] B. Panda, I. Dwivedi, K. Priya, P. B. Karandikar, and P. S. Mandake, "Analysis of aqueous supercapacitor with various current collectors, binders and adhesives," in *2016 Biennial International Conference on Power and Energy Systems: Towards Sustainable Energy (PESTSE)*, Bangalore: IEEE, Jan. 2016, pp. 1–6. doi: 10.1109/PESTSE.2016.7516457.
- [52] Q. Cheng, J. Tang, J. Ma, H. Zhang, N. Shinya, and L.-C. Qin, "Graphene and carbon nanotube composite electrodes for supercapacitors with ultra-high energy density," *Phys. Chem. Chem. Phys.*, vol. 13, no. 39, p. 17615, 2011, doi: 10.1039/c1cp21910c.
- [53] A. G. Pandolfo and A. F. Hollenkamp, "Carbon properties and their role in supercapacitors," *J. Power Sources*, vol. 157, no. 1, pp. 11–27, Jun. 2006, doi: 10.1016/j.jpowsour.2006.02.065.
- [54] L. Xie *et al.*, "Hierarchical porous carbon microtubes derived from willow catkins for supercapacitor applications," *J. Mater. Chem. A*, vol. 4, no. 5, pp. 1637–1646, 2016, doi: 10.1039/C5TA09043A.
- [55] J. Jiang, Y. Li, J. Liu, X. Huang, C. Yuan, and X. W. (David) Lou, "Recent Advances in Metal Oxide-based Electrode Architecture Design for Electrochemical Energy Storage," *Adv. Mater.*, vol. 24, no. 38, pp. 5166–5180, Oct. 2012, doi: 10.1002/adma.201202146.
- [56] P. Forouzandeh, V. Kumaravel, and S. C. Pillai, "Electrode Materials for Supercapacitors: A Review of Recent Advances," *Catalysts*, vol. 10, no. 9, p. 969, Aug. 2020, doi: 10.3390/catal10090969.
- [57] C. Zhao and W. Zheng, "A Review for Aqueous Electrochemical Supercapacitors," *Front. Energy Res.*, vol. 3, May 2015, doi: 10.3389/fenrg.2015.00023.
- [58] T. P. Gujar, W.-Y. Kim, I. Puspitasari, K.-D. Jung, and O.-S. Joo, "Electrochemically Deposited Nanograin Ruthenium Oxide as a Pseudocapacitive Electrode," *Int. J.*

- Electrochem. Sci.*, vol. 2, no. 9, pp. 666–673, Sep. 2007, doi: 10.1016/S1452-3981(23)17102-1.
- [59] K. Kong, J. Hyun, Y. Kim, W. Kim, and D. Kim, “Nanoporous structure synthesized by selective phase dissolution of AlCoCrFeNi high entropy alloy and its electrochemical properties as supercapacitor electrode,” *J. Power Sources*, vol. 437, p. 226927, Oct. 2019, doi: 10.1016/j.jpowsour.2019.226927.
- [60] Y. Ren *et al.*, “Hydrothermal Synthesis of  $\beta$ -Ni(OH)<sub>2</sub> Nanoplates as Electrochemical Pseudocapacitor Materials,” *Int. J. Electrochem. Sci.*, vol. 7, no. 12, pp. 12236–12243, Dec. 2012, doi: 10.1016/S1452-3981(23)16540-0.
- [61] S. Goel, A. K. Tomar, R. K. Sharma, and G. Singh, “Highly Pseudocapacitive NiO Nanoflakes through Surfactant-Free Facile Microwave-Assisted Route,” *ACS Appl. Energy Mater.*, vol. 1, no. 4, pp. 1540–1548, Apr. 2018, doi: 10.1021/acsaem.7b00343.
- [62] M. Aghazadeh, A. Rashidi, M. R. Ganjali, and M. G. Maragheh, “Nickel oxide Nano-Rods/Plates as a High Performance Electrode Materials for Supercapacitors; Electrosynthesis and Evolution of Charge Storage Ability,” *Int. J. Electrochem. Sci.*, vol. 11, no. 12, pp. 11002–11015, Dec. 2016, doi: 10.20964/2016.12.115.
- [63] D.-W. Wang *et al.*, “Fabrication of Graphene/Polyaniline Composite Paper via *In Situ* Anodic Electropolymerization for High-Performance Flexible Electrode,” *ACS Nano*, vol. 3, no. 7, pp. 1745–1752, Jul. 2009, doi: 10.1021/nn900297m.
- [64] C. Zhou, Y. Zhang, Y. Li, and J. Liu, “Construction of High-Capacitance 3D CoO@Polypyrrole Nanowire Array Electrode for Aqueous Asymmetric Supercapacitor,” *Nano Lett.*, vol. 13, no. 5, pp. 2078–2085, May 2013, doi: 10.1021/nl400378j.
- [65] Y. Shi *et al.*, “Nanostructured conductive polypyrrole hydrogels as high-performance, flexible supercapacitor electrodes,” *J Mater Chem A*, vol. 2, no. 17, pp. 6086–6091, 2014, doi: 10.1039/C4TA00484A.
- [66] C. V. Kumar and A. Pattammattel, “Discovery of graphene and beyond,” in *Introduction to Graphene*, Elsevier, 2017, pp. 1–15. doi: 10.1016/B978-0-12-813182-4.00001-5.
- [67] P. Forouzandeh and S. C. Pillai, “Two-dimensional (2D) electrode materials for supercapacitors,” *Mater. Today Proc.*, vol. 41, pp. 498–505, 2021, doi: 10.1016/j.matpr.2020.05.233.
- [68] C. Liu, Z. Yu, D. Neff, A. Zhamu, and B. Z. Jang, “Graphene-Based Supercapacitor with an Ultrahigh Energy Density,” *Nano Lett.*, vol. 10, no. 12, pp. 4863–4868, Dec. 2010, doi: 10.1021/nl102661q.
- [69] T. Kim, G. Jung, S. Yoo, K. S. Suh, and R. S. Ruoff, “Activated Graphene-Based Carbons as Supercapacitor Electrodes with Macro- and Mesopores,” *ACS Nano*, vol. 7, no. 8, pp. 6899–6905, Aug. 2013, doi: 10.1021/nn402077v.

- [70] X. Li and H. Zhu, “Two-dimensional MoS<sub>2</sub>: Properties, preparation, and applications,” *J. Materiomics*, vol. 1, no. 1, pp. 33–44, Mar. 2015, doi: 10.1016/j.jmat.2015.03.003.
- [71] Y. Zheng *et al.*, “Recent advances of two-dimensional transition metal nitrides for energy storage and conversion applications,” *FlatChem*, vol. 19, p. 100149, Jan. 2020, doi: 10.1016/j.flatc.2019.100149.
- [72] O. M. Yaghi and H. Li, “Hydrothermal Synthesis of a Metal–Organic Framework Containing Large Rectangular Channels,” *J. Am. Chem. Soc.*, vol. 117, no. 41, pp. 10401–10402, Oct. 1995, doi: 10.1021/ja00146a033.
- [73] R. R. Salunkhe, Y. V. Kaneti, and Y. Yamauchi, “Metal–Organic Framework-Derived Nanoporous Metal Oxides toward Supercapacitor Applications: Progress and Prospects,” *ACS Nano*, vol. 11, no. 6, pp. 5293–5308, Jun. 2017, doi: 10.1021/acsnano.7b02796.
- [74] K. Zhao *et al.*, “Vertically aligned MnO<sub>2</sub> nanosheets coupled with carbon nanosheets derived from Mn-MOF nanosheets for supercapacitor electrodes,” *J. Mater. Sci.*, vol. 53, no. 18, pp. 13111–13125, Sep. 2018, doi: 10.1007/s10853-018-2562-3.
- [75] M. Naguib *et al.*, “Two-Dimensional Nanocrystals Produced by Exfoliation of Ti<sub>3</sub>AlC<sub>2</sub>,” *Adv. Mater.*, vol. 23, no. 37, pp. 4248–4253, Oct. 2011, doi: 10.1002/adma.201102306.
- [76] M. Naguib *et al.*, “New Two-Dimensional Niobium and Vanadium Carbides as Promising Materials for Li-Ion Batteries,” *J. Am. Chem. Soc.*, vol. 135, no. 43, pp. 15966–15969, Oct. 2013, doi: 10.1021/ja405735d.
- [77] M. Naguib *et al.*, “Two-Dimensional Transition Metal Carbides,” *ACS Nano*, vol. 6, no. 2, pp. 1322–1331, Feb. 2012, doi: 10.1021/nn204153h.
- [78] S. Hajian, D. Maddipatla, B. B. Narakathu, and M. Z. Atashbar, “MXene-based flexible sensors: A review,” *Front. Sens.*, vol. 3, p. 1006749, Oct. 2022, doi: 10.3389/fsens.2022.1006749.
- [79] T. Li *et al.*, “Fluorine-Free Synthesis of High-Purity Ti<sub>3</sub>C<sub>2</sub>T<sub>x</sub> (T=OH, O) via Alkali Treatment,” *Angew. Chem. Int. Ed.*, vol. 57, no. 21, pp. 6115–6119, May 2018, doi: 10.1002/anie.201800887.
- [80] S.-Y. Pang *et al.*, “Universal Strategy for HF-Free Facile and Rapid Synthesis of Two-dimensional MXenes as Multifunctional Energy Materials,” *J. Am. Chem. Soc.*, vol. 141, no. 24, pp. 9610–9616, Jun. 2019, doi: 10.1021/jacs.9b02578.
- [81] J. Guo, Y. Zhao, A. Liu, and T. Ma, “Electrostatic self-assembly of 2D delaminated MXene (Ti<sub>3</sub>C<sub>2</sub>) onto Ni foam with superior electrochemical performance for supercapacitor,” *Electrochimica Acta*, vol. 305, pp. 164–174, May 2019, doi: 10.1016/j.electacta.2019.03.025.

- [82] C. Zhu, C. Pei, H. S. Park, and X. Yu, "Design of 2D/2D heterostructure by coupling cobalt hydroxides with Mxene on nickel foam for high energy density supercapacitors," *J. Alloys Compd.*, vol. 948, p. 169809, Jul. 2023, doi: 10.1016/j.jallcom.2023.169809.
- [83] L. Zhang *et al.*, "Construction of Monolayer Ti<sub>3</sub>C<sub>2</sub>T<sub>x</sub> MXene on Nickel Foam under High Electrostatic Fields for High-Performance Supercapacitors," *Nanomaterials*, vol. 14, no. 10, p. 887, May 2024, doi: 10.3390/nano14100887.
- [84] B. Qiu, W. Hu, D. Zhang, Y. Wang, and H. Chu, "Biomass-derived carbon as a potential sustainable material for supercapacitor-based energy storage: Design, construction and application," *J. Anal. Appl. Pyrolysis*, vol. 181, p. 106652, Aug. 2024, doi: 10.1016/j.jaap.2024.106652.
- [85] X. Tang *et al.*, "Research advances in biomass-derived nanostructured carbons and their composite materials for electrochemical energy technologies," *Prog. Mater. Sci.*, vol. 118, p. 100770, May 2021, doi: 10.1016/j.pmatsci.2020.100770.
- [86] A. Wu, J. Yan, W. Xu, and X. Li, "Fabrication of waste biomass derived carbon by pyrolysis," *Mater. Lett.*, vol. 173, pp. 60–63, Jun. 2016, doi: 10.1016/j.matlet.2016.03.025.
- [87] P. T. Varsha Raveendran and N. K. Renuka, "Hydrothermal synthesis of biomass-derived carbon nanodots: Characterization and applications," *Mater. Chem. Phys.*, vol. 288, p. 126236, Sep. 2022, doi: 10.1016/j.matchemphys.2022.126236.
- [88] L. Qian *et al.*, "Recent development in the synthesis of agricultural and forestry biomass-derived porous carbons for supercapacitor applications: a review," *Ionics*, vol. 26, no. 8, pp. 3705–3723, Aug. 2020, doi: 10.1007/s11581-020-03626-1.
- [89] J. Wang and S. Kaskel, "KOH activation of carbon-based materials for energy storage," *J. Mater. Chem.*, vol. 22, no. 45, p. 23710, 2012, doi: 10.1039/c2jm34066f.
- [90] X.-L. Su *et al.*, "Three-dimensional porous activated carbon derived from loofah sponge biomass for supercapacitor applications," *Appl. Surf. Sci.*, vol. 436, pp. 327–336, Apr. 2018, doi: 10.1016/j.apsusc.2017.11.249.
- [91] J. Deng *et al.*, "Inspired by bread leavening: one-pot synthesis of hierarchically porous carbon for supercapacitors," *Green Chem.*, vol. 17, no. 7, pp. 4053–4060, 2015, doi: 10.1039/C5GC00523J.
- [92] G. Gou, F. Huang, M. Jiang, J. Li, and Z. Zhou, "Hierarchical porous carbon electrode materials for supercapacitor developed from wheat straw cellulosic foam," *Renew. Energy*, vol. 149, pp. 208–216, Apr. 2020, doi: 10.1016/j.renene.2019.11.150.
- [93] M. M. Baig and I. H. Gul, "Conversion of wheat husk to high surface area activated carbon for energy storage in high-performance supercapacitors," *Biomass Bioenergy*, vol. 144, p. 105909, Jan. 2021, doi: 10.1016/j.biombioe.2020.105909.



- [94] I. A. Alsafari, S. Munir, S. Zulfiqar, M. S. Saif, M. F. Warsi, and M. Shahid, "Synthesis, characterization, photocatalytic and antibacterial properties of copper Ferrite/MXene (CuFe<sub>2</sub>O<sub>4</sub>/Ti<sub>3</sub>C<sub>2</sub>) nanohybrids," *Ceram. Int.*, vol. 47, no. 20, pp. 28874–28883, Oct. 2021, doi: 10.1016/j.ceramint.2021.07.048.
- [95] "X-ray Powder Diffraction (XRD)," *Methods*. Accessed: Oct. 09, 2024. [Online]. Available: [https://serc.carleton.edu/msu\\_nanotech/methods/XRD.html](https://serc.carleton.edu/msu_nanotech/methods/XRD.html)
- [96] S. R. Falsafi, H. Rostamabadi, and S. M. Jafari, "X-ray diffraction (XRD) of nanoencapsulated food ingredients," in *Characterization of Nanoencapsulated Food Ingredients*, Elsevier, 2020, pp. 271–293. doi: 10.1016/B978-0-12-815667-4.00009-2.
- [97] "What is Raman Spectroscopy? - HORIBA." Accessed: Oct. 09, 2024. [Online]. Available: <https://www.horiba.com/int/scientific/technologies/raman-imaging-and-spectroscopy/raman-spectroscopy/>
- [98] "[No title found]."
- [99] "What is SEM Analysis and Why Is It Important?" Accessed: Oct. 09, 2024. [Online]. Available: <https://secat.net/sem-analysis-use-importance/>
- [100] M. Shawky, El-Said El-Said El-Shereafy, I. Ahmed, and A. Y. Shenouda, "A Study on Synthesis and Characterization of Some (I -IV -VI) Groups Compounds for Solar Cells Energy Application," 2016, doi: 10.13140/RG.2.2.21918.79685.
- [101] J. B. Condon, *Surface area and porosity determinations by physisorption: measurements and theory*, 1st ed. Amsterdam: Elsevier, 2006.
- [102] P. Majumdar, "Development of Electrodes for Artificial Photosynthetic System," 2017, doi: 10.13140/RG.2.2.21857.71528.
- [103] "Bet - Micromeritics." Accessed: Oct. 09, 2024. [Online]. Available: <https://www.micromeritics.com/bet/>
- [104] "Cyclic Voltammetry - MTX Labs-Electrochemical Devices & Accessories." Accessed: Oct. 09, 2024. [Online]. Available: <https://mtxlabsglobal.com/cyclic-voltammetry/>
- [105] Y. Shi, Y. Luo, W. Li, M. Ni, and N. Cai, "High Temperature Electrolysis for Hydrogen or Syngas Production from Nuclear or Renewable Energy," in *Handbook of Clean Energy Systems*, 1st ed., J. Yan, Ed., Wiley, 2015, pp. 1–19. doi: 10.1002/9781118991978.hces146.
- [106] E. Barsoukov, *Impedance Spectroscopy: Theory, Experiment, and Applications*, 2nd ed. Hoboken: John Wiley & Sons, Incorporated, 2005.
- [107] F. Wang *et al.*, "Facile synthesis SnO<sub>2</sub> nanoparticle-modified Ti<sub>3</sub>C<sub>2</sub> MXene nanocomposites for enhanced lithium storage application," *J. Mater. Sci.*, vol. 52, no. 7, pp. 3556–3565, Apr. 2017, doi: 10.1007/s10853-016-0369-7.

- [108] T. Kesavan, T. Partheeban, M. Vivekanantha, M. Kundu, G. Maduraiveeran, and M. Sasidharan, "Hierarchical nanoporous activated carbon as potential electrode materials for high performance electrochemical supercapacitor," *Microporous Mesoporous Mater.*, vol. 274, pp. 236–244, Jan. 2019, doi: 10.1016/j.micromeso.2018.08.006.
- [109] M. A. A. M. Abdah *et al.*, "Facile synthesis of microwave-etched Ti3C2 MXene/activated carbon hybrid for lithium-ion battery anode," *J. Electroanal. Chem.*, vol. 928, p. 117050, Jan. 2023, doi: 10.1016/j.jelechem.2022.117050.
- [110] D. Yan, L. Liu, X. Wang, K. Xu, and J. Zhong, "Biomass-Derived Activated Carbon Nanoarchitectonics with Hibiscus Flowers for High-Performance Supercapacitor Electrode Applications," *Chem. Eng. Technol.*, vol. 45, no. 4, pp. 649–657, Apr. 2022, doi: 10.1002/ceat.202100585.
- [111] X. Hong *et al.*, "A wheat flour derived hierarchical porous carbon/graphitic carbon nitride composite for high-performance lithium–sulfur batteries," *Carbon*, vol. 170, pp. 119–126, Dec. 2020, doi: 10.1016/j.carbon.2020.08.032.
- [112] A. Arifuzzaman, I. N. Musa, M. K. Aroua, and R. Saidur, "MXene based activated carbon novel nano-sandwich for efficient CO2 adsorption in fixed-bed column," *J. CO2 Util.*, vol. 68, p. 102353, Feb. 2023, doi: 10.1016/j.jcou.2022.102353.
- [113] H. Zhou *et al.*, "MnO2 nanorods/MXene/CC composite electrode for flexible supercapacitors with enhanced electrochemical performance," *J. Alloys Compd.*, vol. 802, pp. 259–268, Sep. 2019, doi: 10.1016/j.jallcom.2019.06.173.
- [114] X.-Q. Lin, Q.-F. Lü, Q. Li, M. Wu, and R. Liu, "Fabrication of Low-Cost and Ecofriendly Porous Biocarbon Using Konjaku Flour as the Raw Material for High-Performance Supercapacitor Application," *ACS Omega*, vol. 3, no. 10, pp. 13283–13289, Oct. 2018, doi: 10.1021/acsomega.8b01718.
- [115] G. Nagaraju, S. M. Cha, and J. S. Yu, "Ultrathin nickel hydroxide nanosheet arrays grafted biomass-derived honeycomb-like porous carbon with improved electrochemical performance as a supercapacitive material," *Sci. Rep.*, vol. 7, no. 1, p. 45201, Mar. 2017, doi: 10.1038/srep45201.
- [116] X. Huang, Y. Huang, J. Zhao, G. Xu, and X. Wang, "Facile design and synthesis of nickel foam@MXene@NiCo layered hydroxides core-sheath nanostructure for high mass-loading of supercapacitors," *Electrochimica Acta*, vol. 461, p. 142657, Sep. 2023, doi: 10.1016/j.electacta.2023.142657.
- [117] J. Guo *et al.*, "Double layers combined with MXene and in situ grown NiAl-LDH arrays on nickel foam for enhanced asymmetric supercapacitors," *Ionics*, vol. 28, no. 6, pp. 2967–2977, Jun. 2022, doi: 10.1007/s11581-022-04520-8.
- [118] Z. Cui *et al.*, "Synthesis and Supercapacitance of Co<sub>3</sub>O<sub>4</sub> Supported on Porous Carbon Derived from Wheat Flour," *ECS J. Solid State Sci. Technol.*, vol. 7, no. 10, pp. M161–M165, 2018, doi: 10.1149/2.0141810jss.



